Do Phenyl Substituents Affect the Properties of Azobenzocrown Derivatives?

Ewa Wagner-Wysiecka*[a,d], Paulina Szulc[a], Elżbieta Luboch[a], Jarosław Chojnacki[b], Dominika Laskowska[a], Paulina Miklaszewska[a] and Paweł Sowiński[c]

[a] Department of Chemistry and Technology of Functional Materials, Faculty of Chemistry, Gdańsk University of Technology, Narutowicza Street 11/12, 80-233 Gdańsk, Poland

[b] Department of Inorganic Chemistry, Faculty of Chemistry, Gdańsk University of Technology, Narutowicza Street 11/12, 80-233 Gdańsk, Poland

[c] Nuclear Magnetic Resonance Laboratory, Faculty of Chemistry, Gdańsk University of Technology, Narutowicza Street 11/12, 80-233 Gdańsk, Poland

[d] Advanced Materials Center, Faculty of Chemistry, Gdańsk University of Technology, Narutowicza Street 11/12, 80-233 Gdańsk, Poland

Abstract: New products of photo- and thermal rearrangements of 19-membered azoxybenzocrown with phenyl substituents in benzene rings in the *para* positions to oligooxyethylene fragments are characterized. The yields of photochemical transformations depend on the solvent. *Para*-hydroxyazocrown is formed with yields over 50% in propan-2-ol. *Ortho*-hydroxyazobenzocrown is obtained with yields up to 70% in toluene/acetic acid mixture. Macrocyclic **Ph-20-ester** is obtained in yield 90% under thermochemical rearrangement conditions. Structure of new hydroxyazobenzocrowns and also atypical product of rearrangements, 20-membered ester, was confirmed by X-ray diffraction analysis. Azophenol⇄quinone–hydrazone tautomeric equilibrium of new hydroxyazobenzocrowns and the influence of metal cations on tautomeric equilibrium was investigated using ^{1}H NMR and UV-Vis spectroscopy in acetonitrile. The highest value of stability constant (logK 7.25) was obtained for strontium complex of *p*-hydroxyazobenzocrown. For the first time *p*-hydroxyazobenzocrown was used as a chromoionophore in the receptor layer of an optical sensor. Comparative analysis with data obtained previously for series 19-membered analogs have shown the influence of the presence of substituents in benzene rings for the course and products distribution of photo- and thermal rearrangement. The effect of substituents was also discussed against the tautomeric equilibrium and metal cation complexation properties.

Introduction

Supramolecular systems for many decades have been a subject of interest in many areas[1] such as, for example, pharmaceutical[2] or food[3] industries. Modern medicine can be also inspired by supramolecular chemistry.[4-6] The properties of macrocyclic compounds, namely the selective molecular recognition of particular guest molecules, make them useful in analytical sciences.[7-9] Macrocyclic compounds, such as crown ethers and other, can be used for the preparation of the selective stationary phases for chromatography and separation techniques,[10-12] new and advanced sensing of various types of analytes.[13-16] Optical sensors based on supramolecular approach are getting more and more recognition due to their simplicity in addition to their accuracy and precision.[17-19] The modification of the skeleton of macrocycles can lead to compounds bearing different functionalities and interesting properties. Among them are azomacrocyclic compounds with azo moiety as a part of macroring.[20-22] They are known from their various applications e.g. molecular devices such as photoswitches.[23,24] Macrocycles in which azobenzene moiety in *o,o′*-positions is linked by oligoether fragment[22,25,26] are often called azobenzocrowns. Their synthetic procedures can use 2,2′-dihydroxyazobenzenes as substrates (Williamson synthesis).[e.g.25-28] Reductive macrocyclization of dinitropodands was also found to be a convenient way of the preparation of azomacrocyclic

compounds.[e.g.27,29] A variety of azobenzocrowns has been obtained in this way in our group[e.g.30-33] and investigated, among the other as ionophores in membrane ion-selective electrodes. In reductive macrocyclization also azoxycompounds are formed. Azoxycompounds, under defined conditions, are known to undergo various transformations, such as Wallach[34,35] or so called photo-Wallach rearrangements.[36,37] It was clearly shown by us[38, 39] that procedures in which azoxymacrocycles were used, as relatively easily and efficiently obtainable substrates, in rearrangement protocols can be an interesting way of the preparation of macrocyclic compounds. Among them are hydroxyazomacrocycles as well as compounds of rather unexpected structure.[38,39] The main aim of the present work was the investigation of the direction of the rearrangements of sterically hindered azoxymacrocycle and characterization of the formed products. In this attempt we have used 19-membered azoxybenzocrown with two phenyl substituents in benzene rings in *para* positions to the oligooxyethylene fragment (*meta* positions to azoxy group), labeled as **Ph-19-Azo-O**.

Results and Discussion

Rearrangement of Ph-19-Azo-O

A number of photochemical experiments leading to rearrangement of 19-membered azoxybenzocrown with phenyl substituents (**Ph-19-Azo-O**) have been carried out in two solvents of different properties: toluene and propan-2-ol. Additionally processes were carried out in the presence of catalytic amounts of acetic acid. Experiments analogous to described earlier for **19-Azo-O**[38] without additional substituents in benzene rings and ***t*-Bu-19-Azo-O**[39] with two bulky *tert*-butyl groups were conducted to compare the effect of the substituents on the rearrangement course. In Scheme 1 the main products of photo- and thermochemical rearrangements of **Ph-19-Azo-O**, namely **Ph-19-*p*-OH**, **Ph-19-*o*-OH**, **Ph-20-ester**, **Ph-19-al** and **Ph-17-*p*-OH** are shown.

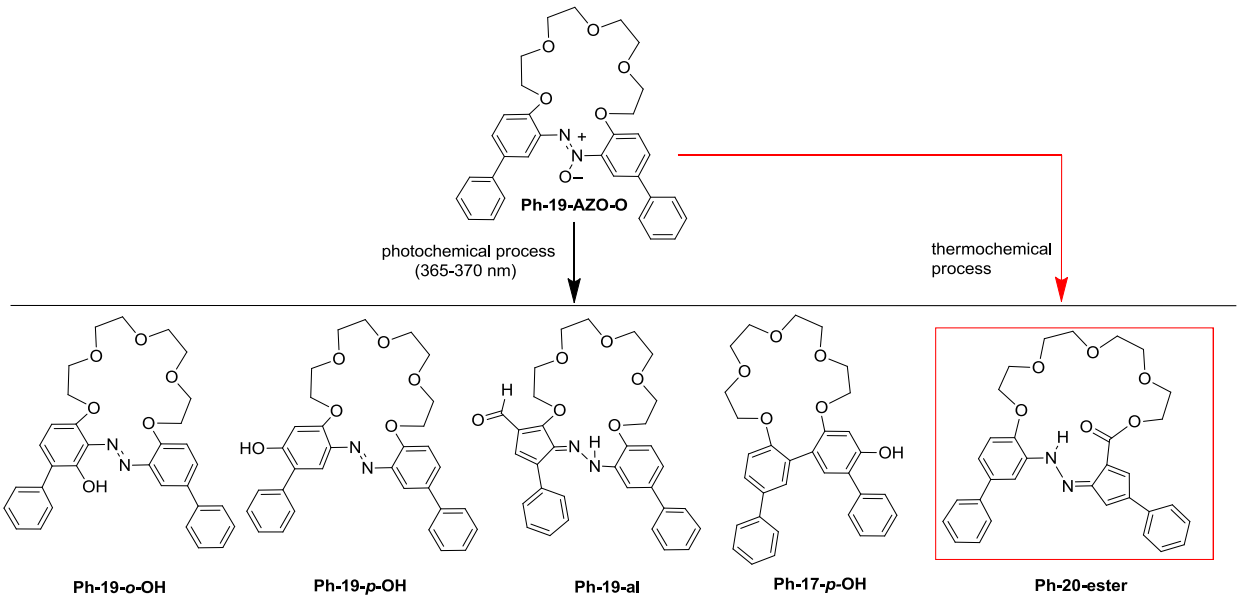

Scheme 1. Products of photochemical and thermal rearrangement of **Ph-19-Azo-O**.

Yields of products of the photochemical transformation of 19-membered azoxycrown **Ph-19-Azo-O** are shown in Figure 2 and given in Experimental (Table 2). The formation of *para*-hydroxyazobenzocrown **Ph-19-*p*-OH** as dominant product (53%) was found in propan-2-ol. *Ortho* isomer was formed in almost 70%, when toluene with a catalytic amount of acetic acid was used as a solvent. Besides hydroxyazobenzocrowns a colorless product - without azo group - **Ph-17-*p*-OH** was formed in all processes, with the highest transformation degree in toluene (14%). This is probably why, among others, the yield of **Ph-19-*p*-OH** is so low in this solvent. Rearrangement leading to formation of **Ph-19-al** and **Ph-20-ester** seems to be favored in toluene with transformation yields ~14% and up to ~8.5%, respectively. In propan-2-ol and its mixture with acetic acid the yield of these products did not exceed 3% (for **Ph-19-al**). **Ph-20-ester** and **Ph-19-al** formation was not observed in toluene/acetic acid mixture. While an effective method of preparation of **Ph-20-ester** is thermochemical rearrangement (yield over 90%). All newly obtained compounds in this work were identified using spectroscopic methods. The respective spectra confirming the structures i.e. ^{1}H NMR, ^{13}C NMR, FT-IR and HR mass spectra are included in the Supplementary Information (Figures S1-S5). The structure of **Ph-19-*p*-OH**, **Ph-19-*o*-OH** and **Ph-20-ester** was also confirmed in a solid state. Nuclear magnetic resonance spectroscopy was used for detailed description of structure of **Ph-17-*p*-OH** and **Ph-20-ester** in solution (*vide infra*).

The course of photochemical rearrangements of 19-membered azoxybenzocrowns, namely the type and amount of products which are formed under UV illumination was compared for **19-Azo-O**, ***t*-Bu-19-Azo-O** and **Ph-19-Azo-O** by analyzing the effect of the presence of substituents in the benzene rings in the *para* position to oligoether moiety. The yield of transformations of 19-membered azoxybenzocrowns to 19-membered *para*- and *ortho*- hydroxyazobenzocrowns and the respective cyclic aldehydes is compared in Figure 1.

From the comparison in Figure 1a it can be concluded that in propan-2-ol the main direction of transformation of azoxybenzocrowns upon UV illumination is formation of *p*-hydroxyazobenzocrowns. Yields of this rearrangement are approx. 50% or higher - comparable in all cases. However the presence of phenyl substituents affect the process resulting in ~10% lower yield in comparison to unsubstituted and *t*-butyl bearing macrocycles. When reaction medium is propan-2-ol in the presence of catalytic amounts of acetic acid then *p*-hydroxyazobenzocrown is obtained with the highest yield for **19-Azo-O** as substrate (Figure 1b). In this medium preferential formation *o*-hydroxyazobenzocrowns, with excellent yield for *t*-butyl bearing crown, was found. The presence of acetic acid favors the formation of *o*-hydroxyazobenzocrowns also in toluene (Figure 1c). In this solvent process is slightly more efficient for phenyl bearing substrate **Ph-19-Azo-O**. In toluene (Figure 1d) the highest yield of rearrangement towards *o*-hydroxyazobenzocrown was observed for ***t*-Bu-19-Azo-O**.

While the formation of hydroxyazocompounds from azoxyderivatives under UV illumination is predictable, some other atypical compounds were isolated and identified. Among them are macrocyclic aldehydes (blue formulas in the frame in Figure 1). Compounds of this type were found in reaction mixtures of all 19-azoxybenzocrowns used as substrates, when the process was carried out in propan-2-ol and toluene (Figure 1a and Figure 1d). The yield of formation of 19-membered aldehyde was relatively the highest in toluene for unsubstituted **19-Azo-O** and for **Ph-19-Azo-O.** In all other cases no or almost traces of aldehydes were isolated.

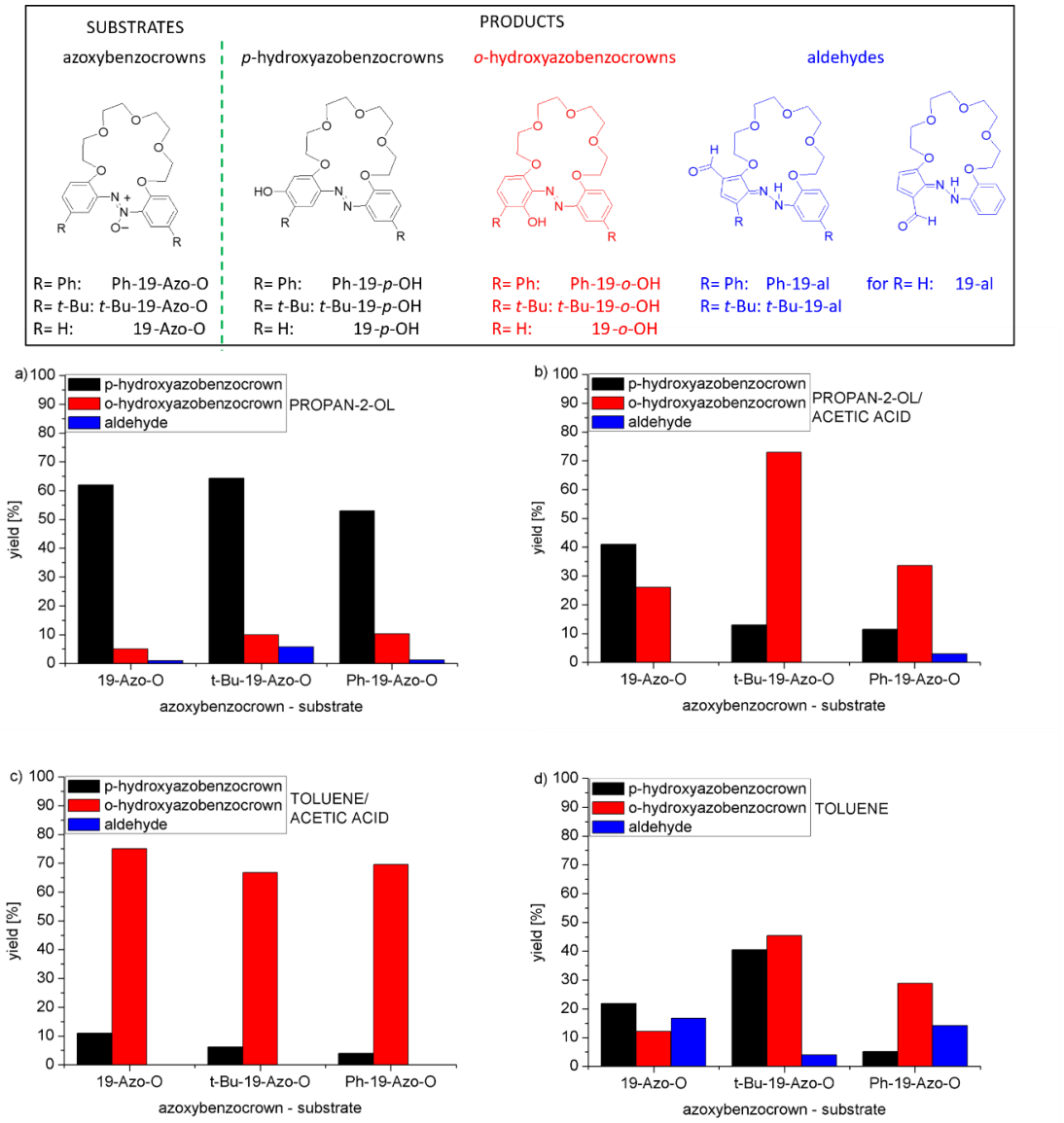

Figure 1. The comparison of the yield of the formation of the colored 19-membered crowns in photochemical rearrangement of 19-membered azoxybenzocrowns: **19-Azo-O**[38], ***t*-Bu-19-Azo-O**[39] and **Ph-19-Azo-O**.

Photo illumination process causes the increase of temperature of reaction mixtures. To prove that UV light is the main factor leading to the transformations of azoxybenzocrowns, here **Ph-19-Azo-O**, the last was heated in darkness in toluene at 80 °C. No rearrangement products were detected under these conditions. However, when **Ph-19-Azo-O** is heated in darkness without a solvent at 155-160 □C thermal rearrangement occurs and **Ph-20-ester** is formed as the main product (~90% yield). Similar results were obtained for the photo- and thermal rearrangement of ***t*-Bu-19-Azo-O**.[39] Under analogous conditions **19-Azo-O** does not undergo rearrangement. 20-membered esters (Table 1) were found in reaction mixtures only in case of transformations of *para*-substituted azoxybenzocrowns **Ph-19-Azo-O** and ***t*-Bu-19-Azo-O.**[38] However the yield did not exceed 8.4% - the highest yield obtained for **Ph-19-Azo-O**. It was found that when the *para* position is unoccupied, one of the rearrangement products is 21-membered crown **21-*o'*-OH**.[38] The highest yield of **21-*o'*-OH** - 37% - was found for photochemical process carried out in xylene. In toluene and propan-2-ol this macrocycle was formed with 28 and 32% yield, respectively. In the presence of acetic acid the yield was lower.
Comparison of the yield of transformations leading to 20-membered esters for **Ph-19-Azo-O** and ***t*-Bu-19-Azo-O** is shown in Table 1.

Tautomeric equilibrium in solution

Tautomeric equilibrium of hydroxyazobenzocrowns of different macrocycle size has been studied by us to different degrees[27,38-41] (Scheme 2).

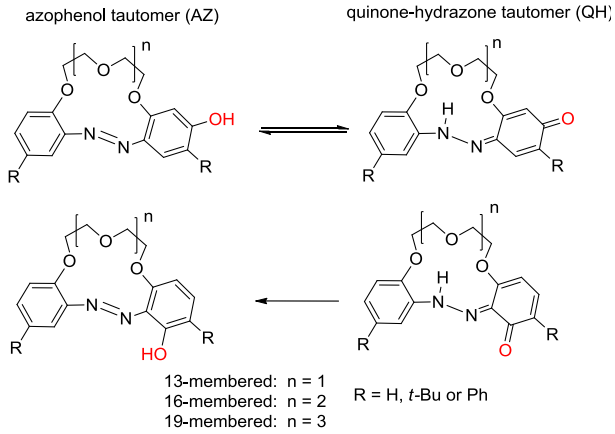

Scheme 2. General presentation of azophenol⇄quinone-hydrazone tautomeric equilibrium of hydroxyazobenzocrowns[27, 38-41].

Table 1. Comparison of the photo- and thermochemical rearrangement transformations of 19-membered azoxybenzocrowns leading to the formation of 21-hydroxyazobenzocrown **21-*o'*-OH** and 20-membered ester derivatives ***t*-Bu-20-ester** and **Ph-20-ester**

Substrate	**19-Azo-O**[38]	***t*-Bu-19-Azo-O**[39]	**Ph-19-Azo-O**
Photo rearrangement			
Product	**21-*o'*-OH** 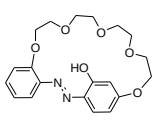	***t*-Bu-20-ester** 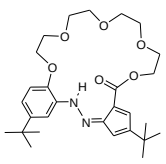	**Ph-20-ester** 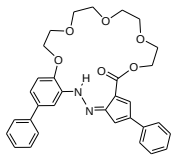
[% yield]			
toluene	28.3	3.5	8.4
toluene acetic/acid	6.0	not detected	not detected
propan-2-ol	32.0	7.1	1.4
propan-2-ol/acetic acid	16.0	not detected	0.7
Thermal rearrangement (solvent free conditions)			
	no product	82	88

Recently, we have concentrated on the more detailed studies of 19-membered compounds.[38,39] Here, we focus on the effect of the presence of aromatic substituents and comparison with results obtained earlier for unsubstituted and *t*-butyl bearing macrocycles.[38,39] Tautomeric equilibrium was studied in solution in solvents of various properties - also in the presence of

acid or base - using well proven[42-44] for this purpose spectroscopic methods: ^{1}H NMR spectroscopy and UV-Vis absorption and emission spectroscopy.

Ph-19-*p*-OH

In acetonitrile-d_3 the quinone-hydrazone (QH) tautomer (77% under ^{1}H NMR spectra registration conditions) of **Ph-19-*p*-OH** is predominant. In ^{1}H NMR spectrum the most characteristic signals for quinone-hydrazone tautomer are peaks at 6.07, 8.04 and 11.87 ppm (cf. Figure S1a). In acetone-d_6 QH form is present in 81% (Figure S1b).
The contribution of tautomers, estimated from ^{1}H NMR spectra (at ~10^{-2} M), for 19-membered *p*-hydroxyazobenzocrowns, namely **19-*p*-OH**, ***t*-Bu-19-*p*-OH** and **Ph-19-*p*-OH** is shown in Figure 2 and listed in Table S1. Tautomeric equilibrium in solution depends on several factors,[45-48] including obviously the structure of the molecule and the properties of its chemical environment such as solvent type, pH, the presence of ionic species (e.g. metal salts) or temperature. For 19-membered *p*-hydroxyazobenzocrowns we have recently postulated[38,39] that in polar solvents such as acetonitrile and DMSO, differing in hydrogen-bonding affinity, the contribution of tautomers seems to be also connected with the presence of substituents in benzene rings. Comparing the properties of *p*-hydroxyazobenzocrown **19-*p*-OH** with its derivatives ***t*-Bu-19-*p*-OH** or **Ph-19-*p*-OH** (Figure 2) it is seen that in highly dipolar, aprotic DMSO (acceptor of hydrogen bond) azophenol form is dominating. It can be explained by the stabilization of this form by the crown-solvent hydrogen bonded system. In dipolar and aprotic acetonitrile the contribution of azophenol tautomer is lower.

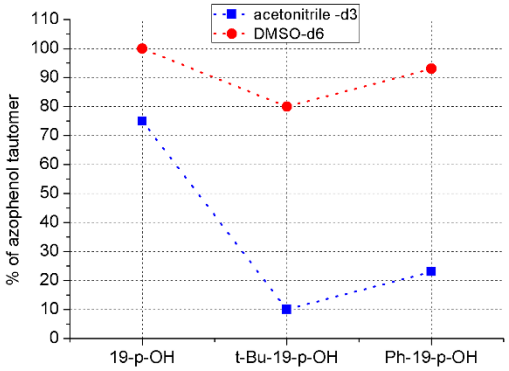

Figure 2. The effect of the substituents on tautomeric equilibrium of 19-membered *p*-hydroxyazobenzocrowns in acetonitrile-d_3 and DMSO-d_6 (on the basis of ^{1}H NMR measurements at ~10^{-2} M).

It might be connected with the hydrogen-bonding properties of this solvent. In studied here derivatives flat phenyl rings affect tautomeric equilibrium less than *t*-butyl groups. As the electronic effects of substituents are relatively comparable (both are defined as weak EDGs), the steric effect of bulky alkyl substituents can be postulated here. Tautomeric equilibrium of **Ph-19-*p*-OH** at lower concentrations (~10^{-5} M) was investigated by UV-Vis absorption and emission spectroscopy. The position of absorption bands of **Ph-19-*p*-OH** is, as can be expected, affected by the properties of solvent. The spectral pattern is also connected with the distribution of tautomers in particular solvent (Figure 3a, Figure 4a, Table S2). In polar and protic methanol as well as in water containing solvent mixtures (acetonitrile and DMSO) the absorption band of quinone-hydrazone tautomer is red shifted compared to dichloromethane or pure acetonitrile. Due to spectral characteristics, the color of solutions of **Ph-19-*p*-OH** in different solvents is not spectacularly different. Only in DMSO and its mixture with water the yellow shade is brighter (Figure S6). In DMSO and its mixture with water azophenol tautomer is dominating, which is in agreement with results obtained from ^{1}H NMR experiments. Water, as protic and hydrogen-bonding solvent, in mixture with acetonitrile, similarly as methanol itself, increases the azophenol tautomer contribution under UV-Vis absorption spectra registration conditions (Figure 4b).

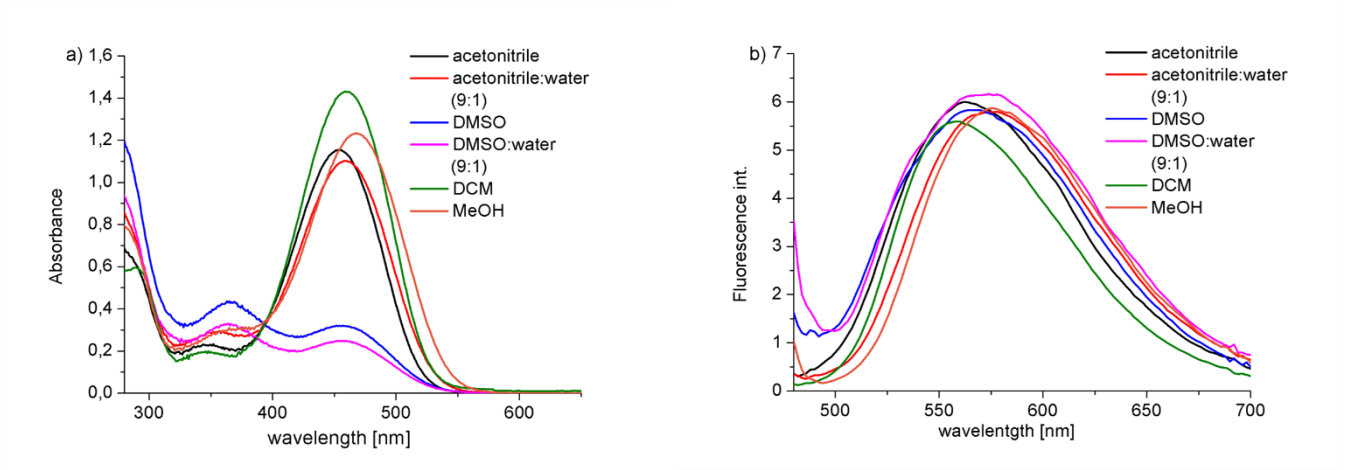

Figure 3. a) UV-Vis absorption and b) emission spectra of **Ph-19-*p*-OH** ($4.0 \cdot 10^{-5}$ M) in solvents of various properties.

This is less seen in DMSO, probably due to the competing effect of polar solvents. Azophenol tautomers are known to be non-fluorescent and the observed fluorescence is reported to be solely connected with the presence of quinone-hydrazone form.[49-51] The position of emission band coming from fluorescent quinone-hydrazone tautomer of **Ph-19-*p*-OH** (fluorescence quantum yield 0.183 in acetonitrile) is located in narrow spectral range: between ~570 and ~590 nm depending on the type of solvent (Figure 3b, Figure 4a and Table S2).

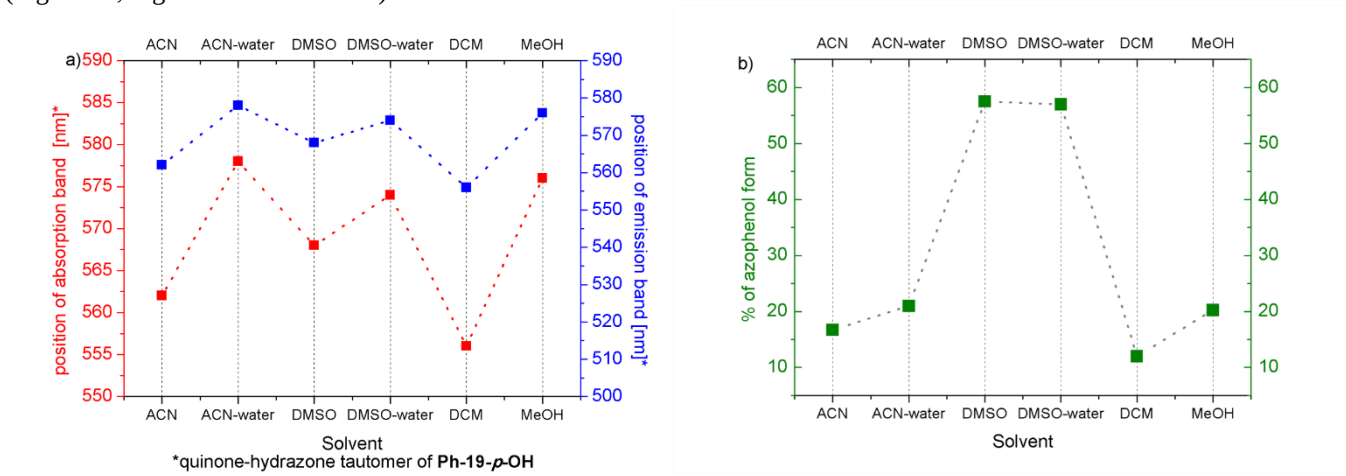

Figure 4. a) The comparison of the position of absorption and emission bands of quinone-hydrazone tautomer of **Ph-19-*p*-OH** and b) the contribution [%] of azophenol form in dependence of solvent properties.

Tautomeric equilibrium of 19-membered hydroxyazobenzocrowns was found to be concentration dependent.[38,39] The contribution of tautomers of **Ph-19-*p*-OH** under UV-Vis spectra registration at concentration ca. 10^{-4} M is listed in Table S3. At lower concentrations where intermolecular interactions are weaker, tautomeric equilibrium is shifted towards quinone-hydrazone form (acetonitrile and DMSO are compared with results from ^{1}H NMR experiments, cf. Table S1).
This is in agreement with results obtained previously for **19-*p*-OH**[38] and ***t*-Bu-19-*p*-OH**.[39] Tautomeric equilibrium of *p*-hydroxyazobenzocrowns of various macroring size is pH sensitive.[38-40,52] The presence of acid shifts tautomeric equilibrium towards protonated azophenol form, whereas in basic environment deprotonated form is dominating. The color change of the solution of **Ph-19-*p*-OH** caused by the presence of acid/base in various solvents is shown in Figure S6. Color change of **Ph-19-*p*-OH** from yellow (long wavelength absorption maximum at 453 nm) is a result of the acid or base induced shift of the absorption band in the electronic spectra. In acidic acetonitrile the main absorption band of protonated azophenol form is observed at 530 nm, which corresponds to the purple color of solution.
In the presence of *tetra-n*-butylammonium hydroxide absorption maximum is observed at 482 nm, which is responsible for orange color of acetonitrile solution and corresponds to ionized quinone-hydrazone tautomer (cf. Figure S7). ^{1}H NMR spectra of **Ph-19-*p*-OH** registered in the presence of *p*-toluenesulfonic acid (Figure S8a) and *tetra-n*-butylammonium hydroxide (Figure S8b) confirm the above mentioned statement, i.e. the formation of protonated azophenol form in the acidic and deprotonated quinone-hydrazone form in basic acetonitrile solution.

Ph-19-*o*-OH

Similarly to previously reported by as results for *o*-hydroxyazobenzocrowns[38-41,52] **Ph-19-*o*-OH** in solution also exists in azophenol form, which is confirmed by ^{1}H NMR spectra registered in acetonitrile-d_3 and DMSO-d_6 (Figure S2a and S2b). In acidic or basic acetonitrile protonated (downfield shift of signal of protons) or deprotonated azophenol (upfield proton signals) forms are present (Figure S9). UV-Vis spectra registered upon titration of acetonitrile solution of **Ph-19-*o*-OH** with *p*-toluenesulfonic acid and *tetra*-*n*-butylammonium hydroxide are shown in Figure S10. Solutions of protonated and deprotonated forms are purple with absorption bands in UV-Vis spectra located at ~ 550 nm. The presence of alkyl (*t*-Bu) or aryl (phenyl) substituents has no effect on the azophenol⇄quinone-hydrazone tautomeric equilibrium of *o*-hydroxyazobenzocrowns.

Metal cation complexation studies

The affinity of **Ph-19-*p*-OH** and **Ph-19-*o*-OH** for metal cations was investigated by spectroscopic methods, namely ^{1}H NMR, UV-Vis absorption and emission spectroscopy. Obtained results were compared with metal cation complexation properties of previously investigated 19-membered crowns **19-*p*-OH** and ***t*-Bu-19-*p*-OH** and their *ortho* isomers.

Ph-19-*p*-OH

UV-Vis absorption spectra of **Ph-19-*p*-OH** registered in acetonitrile show changes in the presence of alkali and alkaline earth metal perchlorates. In most cases the decrease of the intensity of the main band at 453 nm is observed (Figure S11). No spectral changes are observed for lithium perchlorate. For alkaline earth metal perchlorates: calcium, strontium and barium, interaction with metal cations results with hypsochromic spectral shift of 20, 15 and 8 nm respectively (Figure S11). Stability constant values (logK) of 1:1 complexes of **Ph-19-*p*-OH** with metal perchlorates obtained from UV-Vis titration experiments are shown in Figure 5 (blue triangles) and collected in Table S4. The highest value of stability constant was obtained for the strontium complex of **Ph-19-*p*-OH**. In acetonitrile the presence of metal perchlorates, similarly to investigated earlier 19-membered *p*-hydroxyazobenzocrowns[38,39], shifts azophenol⇄quinone-hydrazone tautomeric equilibrium towards azophenol tautomer.

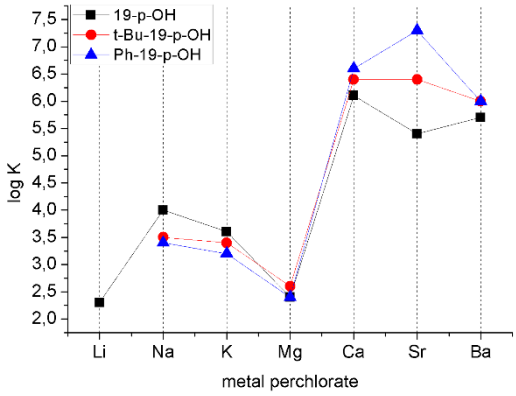

Figure 5. The comparison of the stability constant values (logK) of 1:1 complexes of 19-membered *p*-hydroxyazobenzocrowns: **19-*p*-OH**,[38] ***t*-Bu-19-*p*-OH**[39] and **Ph-19-*p*-OH** with alkali and alkaline metal perchlorates in acetonitrile.

The change of tautomeric equilibrium upon metal cation complexation is confirmed by ^{1}H NMR spectra. Change of the ^{1}H NMR spectrum caused by the presence of metal perchlorates is exemplified by the spectra registered in the presence of sodium perchlorate in acetonitrile-d_3 (Figure 6). A signal characteristic for azophenol tautomer, which is observed at 6.77 ppm, shifts to 6.88 ppm in sodium complex. Full range ^{1}H NMR spectra of **Ph-19-*p*-OH** registered in acetonitrile-d_3 in the presence of sodium perchlorate are shown in Figure S12. Only in the case of magnesium perchlorate the character of changes, both in absorption UV-Vis spectra (Figure S11d) and ^{1}H NMR spectrum, is different (Figure S13). The presence of absorption band at longwave side of spectrum of **Ph-19-*p*-OH** upon titration with magnesium perchlorate in acetonitrile might suggest that magnesium is complexed by both quinone-hydrazone and azophenol tautomers. This finds confirmation in the ^{1}H NMR spectrum of **Ph-19-*p*-OH** registered in equimolar amount and 10-fold excess of magnesium perchlorate in acetonitrile-d_3 (Figure S13). In the presence of magnesium perchlorate signals of Ar-O-C$\underline{H_2}$- protons labeled as 1 and 1' (Table S5) are downfield shifted and observed as triplet at 4.40 ppm (+0.06 ppm in relation to "free" crown) in the presence of equimolar

amount of magnesium salt. In 10-fold excess of magnesium perchlorate signals of oligoether linkage labeled as 1,1' are observed as two separate triplets at 4.44 and 4.41 ppm. Upon complexation downfield shift of signal of aromatic proton of benzene ring with hydroxy group labeled as A (Table S5) is observed. A signal of N-H proton shifts to higher ppm values with increasing amount of magnesium perchlorate. This might suggest that the presence of magnesium cation and its complexation affect the strength of the intramolecular hydrogen bond. In Figure 5 the comparison of the stability constant values of 19-membered *p*-hydroxyazobenzocrowns: **19-*p*-OH**,[38] ***t*-Bu-19-*p*-OH**[39] and **Ph-19-*p*-OH** is presented. The effect of substituents in benzene rings in *para* position to oligoether moiety is well seen. Higher values of stability constant for alkali metal complexes are for unsubstituted *p*-hydroxyazobenzocrown **19-*p*-OH**. Moreover, this is the only case where changes in UV-Vis spectra in the presence of lithium perchlorate are observed. For crowns bearing substituents in *para* positions lithium presence does not affect spectra. On the other hand, stability constants of complexes of this macrocycle with alkaline metal perchlorates are the lowest among investigated *p*-hydroxyazobenzocrowns.

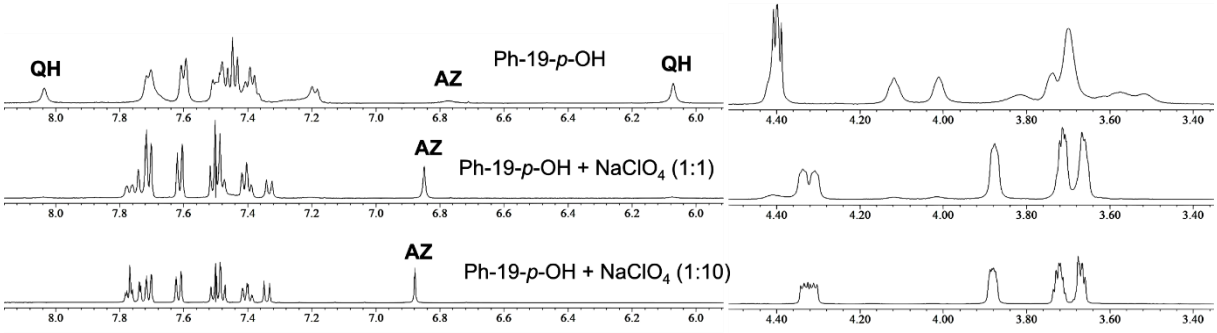

Figure 6. Partial ^{1}H NMR spectra of **Ph-19-*p*-OH** (4.8×10^{-3} M) registered in the presence of sodium perchlorate (acetonitrile-d_3). The most characteristic signals of protons for quinone-hydrazone and azophenol tautomers are marked as QH and AZ.

The presence of substituents, namely *t*-butyl or phenyl, in benzene rings increases the affinity towards alkaline metal cations with highest value of stability constant for strontium complex for **Ph-19-p-OH**. This may be caused by the change of the molecular cavity size affected by the presence of the substituents. Bulky *t*-butyl residues and, most importantly, rigid phenyl rings make *p*-hydroxyazobenzocrowns more preorganized for alkaline metal cations.

Ph-19-*p*-OH as predominantly existing in quinone-hydrazone form, similarly to previously investigated *p*-hydroxyazobenzocrowns, is fluorescent (cf. Figure 3b). The quenching of fluorescence is observed upon titration with all investigated alkali and alkaline earth metal perchlorates. It is contrary to previously investigated 19-membered *p*-hydroxyazobenzocrowns: **19-*p*-OH** and ***t*-Bu-19-*p*-OH** for which the presence of magnesium perchlorate caused the increase of fluorescence intensity. Moreover, the quenching of fluorescence of **Ph-19-*p*-OH** by magnesium perchlorate is additionally connected with a bathochromic shift of emission band of 18 nm. The change of emission spectra of **Ph-19-*p*-OH** caused by metal perchlorates is shown in Figure S14. Stability constant values (logK) of 1:1 complexes obtained from fluorescence titration are listed in Table S4. Values of stability constants calculated from emission titration experiments are lower than the analogous values obtained from absorption spectra (Figure 7a). However the general trend in the strength of binding of metal cation is similar both in the ground and excited state: higher values are obtained for complexes of alkaline earth metal perchlorates. The quenching of fluorescence by metal perchlorates was also characterized by determination of Stern-Volmer constants. Stern-Volmer constants estimated from titration experiments are shown as $\log K_{SV}$ in Figure 7b. From the comparison of data shown in Figures 7a and Figure 7b it can be seen that the trend of affinity towards particular metal perchlorate for **Ph-19-*p*-OH** is additionally in agreement with the tendency to quenching of fluorescence. It means that quenching of fluorescence can be connected with the formation of a complex with metal cations acting as quenchers and can be ascribed as static quenching of fluorescence. This may be connected, as postulated for ***t*-Bu-19-*o*-OH**,[39] with the engagement of one of the nitrogen atoms in complex formation. Signals of protons of oligoether linkage are more equivalent than in the spectrum of uncomplexed crown, which in turn may suggest symmetrical mode of complexation of sodium cation. For alkaline earth metal perchlorates changes upon UV-Vis titrations are observed – negligible for magnesium, but significant for calcium, strontium and barium perchlorates (Figure S15).

Ph-19-*o*-OH

Metal cation affinity of **Ph-19-*o*-OH** was investigated in acetonitrile using UV-Vis absorption and ^{1}H NMR spectroscopy. Upon titration with investigated alkali metal perchlorates significant spectral changes are observed only for sodium perchlorate. Stability constant values (logK) of 1:1 complexes of 19-membered *o*-hydroxyazobenzocrowns with sodium are comparable.

The values 3.51,[38] 3.45[39] and 3.40 for **19-*o*-OH**, ***t*-Bu-19-*o*-OH**, **Ph-19-*o*-OH**, respectively, can indicate the change of the molecular cavity size resulting in slight decrease of crown-sodium affinity caused by the presence of substituents in benzene rings. Similarly to investigated earlier 19-membered analogs, ^{1}H NMR spectrum of **Ph-19-*o*-OH** registered in the presence of sodium perchlorate (acetonitrile-d_3) shows shifting of signal of OH proton towards lower ppm values, which points out lowering the intramolecular hydrogen bond (Figure 8).
The general affinity towards metal cations is in accordance with the results obtained for **19-*o*-OH**[38] and ***t*-Bu-19-*o*-OH**.[39] However it is seen that the binding strength of alkaline earth metal cations is affected by the presence of substituents in benzene rings. The obtained stability constant values (logK) of 1:1 complexes with metal perchlorates are collected in Table S4 and comparison of the binding constants of complexes of 19- membered *o*-hydroxyazobenzocrowns with alkaline earth metal perchlorates in acetonitrile is shown in Figure 9a. From this comparison it can be assumed that the molecular cavity is the smallest in the case of **19-*p*-OH.**

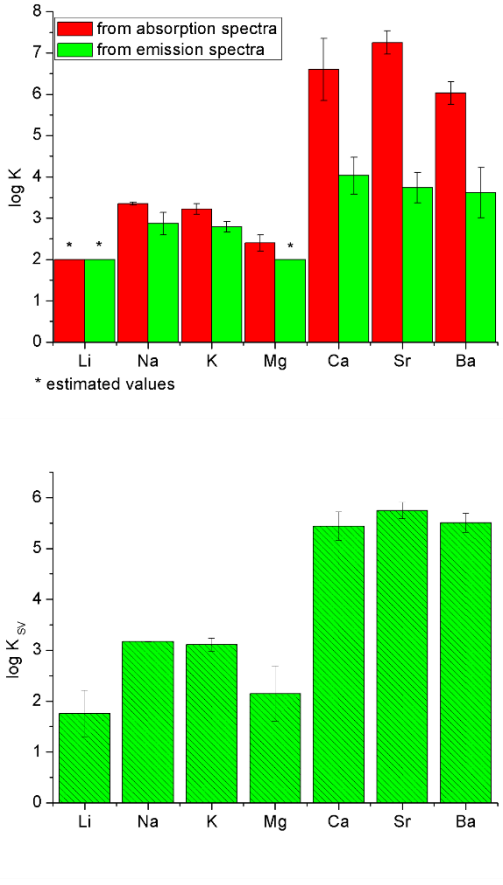

Figure 7. a) The comparison of the values of the stability constants (logK) of 1:1 complexes of **Ph-19-*p*-OH** with metal perchlorates obtained from absorption and emission spectral data in acetonitrile b) the values of Stern-Volmer constants- given as log K_{SV} - obtained for **Ph-19-*p*-OH** in acetonitrile.

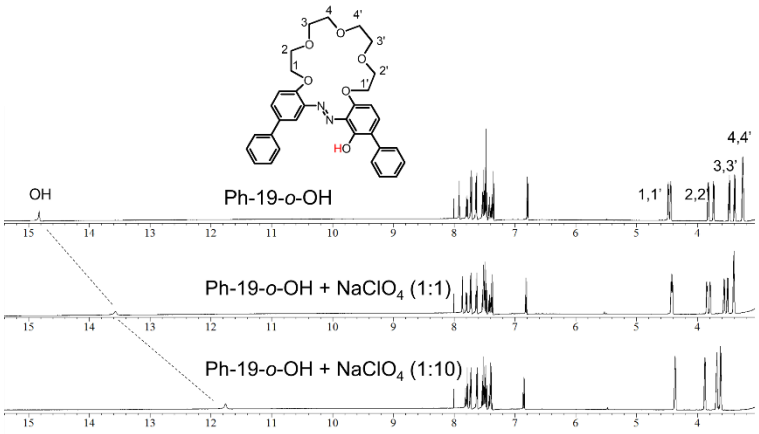

Figure 8. ^{1}H NMR spectra of **Ph-19-*o*-OH** (6.7×10^{-3} M) registered in the presence of equimolar and 10-fold excess of sodium perchlorate (acetonitrile-d_3).

The evidence might be that the highest value of stability constant was found for the smallest metal cation - calcium and the lowest - for the barium cation of the highest ion diameter. On the other hand, the highest value of stability constant for the barium complex was obtained for ***t*-Bu-19-*o*-OH**. The presence of phenyl substituents in **Ph-19-*o*-OH** probably affects molecular cavity size, which is observed as lowering of the selectivity towards alkaline earth metal cations. The effect of the substituents is also seen when comparing the strength of the intramolecular hydrogen bonding, estimated by comparison of the chemical shift of signal of OH proton (Figure 9b) in ^{1}H NMR spectra registered in acetonitrile-d_3. The strongest hydrogen bond is for ***t*-Bu-19-*o*-OH,**[39] next for **Ph-19-*o*-OH** and weaker for **19-*p*-OH**.[38]

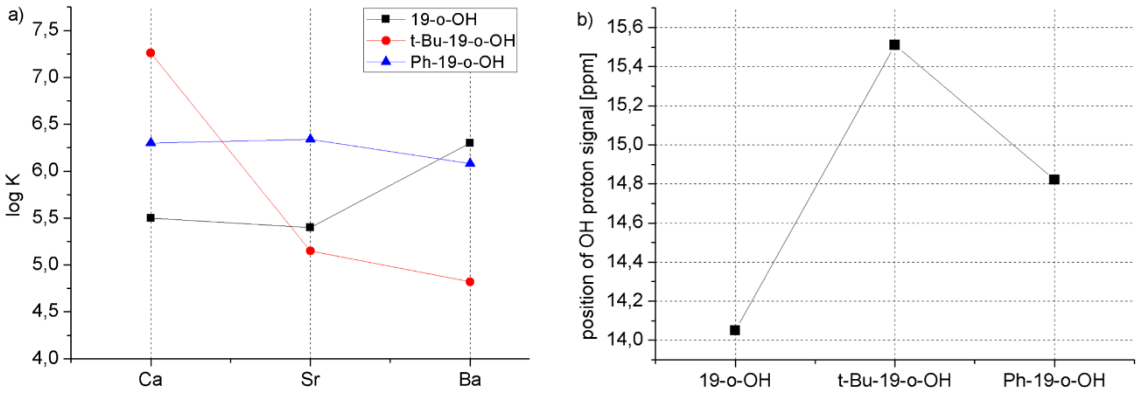

Figure 9. a) Comparison of stability constant values (logK) of complexes of 19-membered *o*-hydroxyazobenzocrowns **19-*o*-OH**,[38] ***t*-Bu-19-*o*-OH**[39] and **Ph-19-*o*-OH** with alkaline earth metal perchlorates in acetonitrile b) comparison of the position of signal of proton of OH group in ^{1}H NMR spectra of **19-*o*-OH**,[38] ***t*-Bu-19-*o*-OH**[39] and **Ph-19-*o*-OH** registered in acetonitrile-d_3.

Description on X-ray structures of Ph-19-*p*-OH, Ph-19-*o*-OH, Ph-20-ester

Detailed data on crystal structure are given in Experimental Section and Supplementary Information of this article. Compound **Ph-19-*p*-OH** in solid state gave two types of crystals, being different polymorphic forms, which were studied using X-ray diffraction analysis (Figure 10).

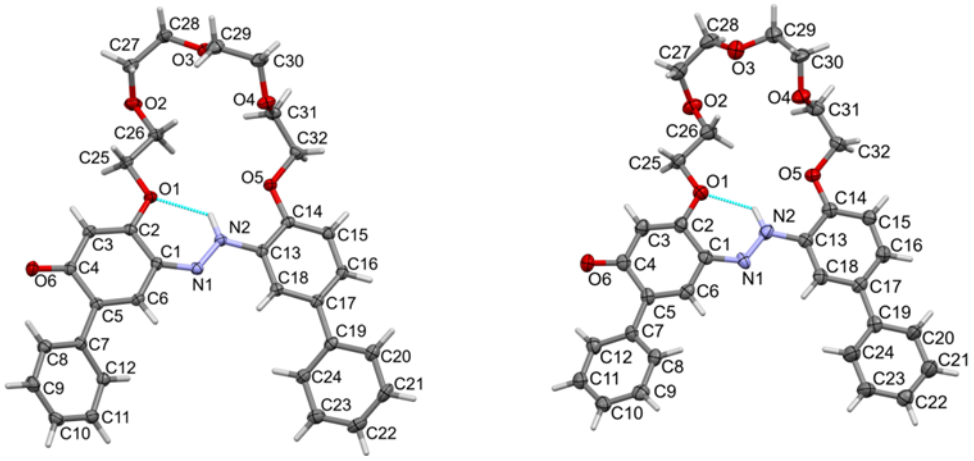

Figure 10. Molecular views of: a) **Ph-19-*p*-OH(1)** (right) and b) **Ph-19-*p*-OH(2)** (left), showing atom labelling scheme. In the case of **Ph-19-*p*-OH(2)**, one molecule was arbitrally selected from the two symmetry independent molecules in the structure. Intramolecular hydrogen bonding drawn as the dashed cyan line. Displacement ellipsoids drawn at 50% probability level. Selected bond lengths (Å) and angles (°): a) C4-O6 1.2415 (17), N1-N2 1.3158 (17), C1-N1 1.3189 (18), N2-C13 1.4038 (18), C2-O1-C25 117.77 (10); b) C4-O6 1.260 (10), N1-N2 1.337 (9), C1-N1 1.319 (10), N2-C13 1.400 (10), C2-O1-C25 117.3 (6). For torsions in the ether linkers see Table S7.

The basic features of molecules in both structures are similar. Relatively short C4-O6 of ca 1.25Å (labelled as C36-O12 in the second symmetry independent molecule in the second polymorph, see cif. file) and long N1-N2 (or N3-N4) bond lengths suggest that the quinone-hydrazone tautomer is dominating in the solid state. Additional stabilization of the molecules is due to intramolecular 6-membered cyclic hydrogen bonding $S(6)$, self type motif. Details on the hydrogen bonding system are collected in Table S6.

First polymorph **Ph-19-*p*-OH(1)** forms needle, red crystals, with symmetry of the monoclinic system, the space group $P2_1/n$ (no. 14). Asymmetric unit contains one molecule and the whole unit cell is built from four molecules, Z = 4. Torsion (dihedral) angles between linked 6-membered rings are relatively wide and different being equal to 25.93□ for rings C1-C6 and C7-C12, and -31.32□ for C13-C18 and C19-C24. For torsions in the ether linkers see Table S7.

The second polymorph **Ph-19-*p*-OH(2)** is also refined in the monoclinic system with four molecules in the unit cell. Nevertheless, space group $P2_1$ (no. 3) lacks a center of symmetry, so the asymmetric unit contains two symmetry independent molecules. Only one of the independent molecules for the second polymorph is shown in Figure 10. The two independent molecules in polymorph 2 differ in torsion angles of the twist of 6-membered rings and in conformation of the ether linker. In both molecules, three phenyl rings are almost coplanar with the rest of the molecule and the last 6-membered ring is inclined 25-35 degree to the mean plane (Figure S16). More precisely: dihedral angles in the first molecule are 25.30□ for rings C1-C6 and C7-C12, and 2.29□ between rings C13-C18 and C19-C24. For the second molecule we found: 33.93□ between rings C33-C38 and C39-C44 and 3.87□ between rings C45-C50 and C51-C56. Side views on molecules from polymorphs of Ph-19-p-OH are shown in Figure S17. Compound **Ph-20-ester** also forms needle, red crystals, but with symmetry of the orthorhombic system, the space group *Pccn* (no. 56). Asymmetric unit contains one molecule, and the unit cell is built from eight molecules, Z = 8. Most of the bond lengths and angles are not unusual (Figure 11). Bonds C2-C3 and C4-C5 are slightly shorter than other bonds in the 5-membered ring, as expected. Moreover, bond C1-N1 is shorter than N2-C13 indicating the double character of the first one. Carbonyl bond C6-O6 is short, too. Bond length N1-N2 is similar to the one found in **Ph-19-*p*-OH**. This time we find 7-membered cyclic intramolecular (self) hydrogen bonding, *S*(7). The ether linker is more bent than in the case of **Ph-19-*p*-OH**, for details see Table S6 and Table S7. Compound **Ph-19-*o*-OH** (Figure 12), forms needle, red crystals, obeying the $P2_1/c$ space group symmetry (monoclinic). Asymmetric unit contains one molecule, so four molecules are present in the unit cell, Z=4. Bond lengths and angles lay rather in the expected ranges. Most evident difference in molecular conformation is the *trans* location of polyether linker ends in ring-N=N-ring moiety. This may be caused by formation of strong OH...N hydrogen bonding between hydroxy and diazo groups, which was not possible in *para*-OH substituted isomers. Detailed information of hydrogen bonds and torsion angles list can be found in Table S6 and Table S7.

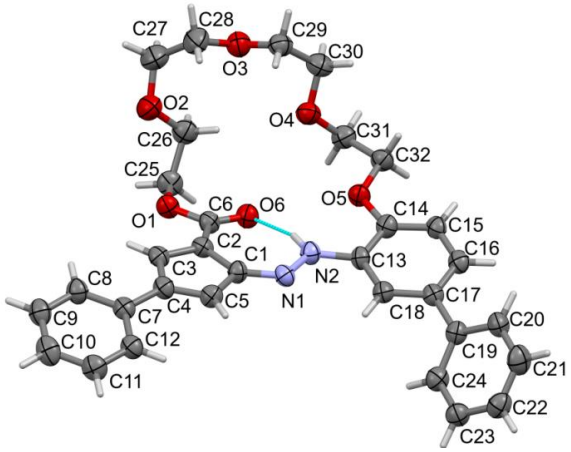

Figure 11. Molecular view of **Ph-20-ester** showing atom labelling scheme. Intramolecular hydrogen bonding drawn as the dashed cyan line. Displacement ellipsoids drawn at 50% probability level. Selected bond lengths (Å) and angles (°): O6-C6 1.225 (5), O1-C6 1.350 (5), N1-N2 1.326 (5), C1-N1 1.324 (5), N2-C13 1.411 (5), C1-N1-N2 119.8 (3), C1-C2-C6 129.1 (4), C2-C6-O6 126.0 (4), C1-C2-C3 106.2 (3), C2-C3-C4 110.8 (4), C3-C4-C5 106.6 (4), C4-C5-C1 109.6 (4). For torsions in the linker ether see Table S7.

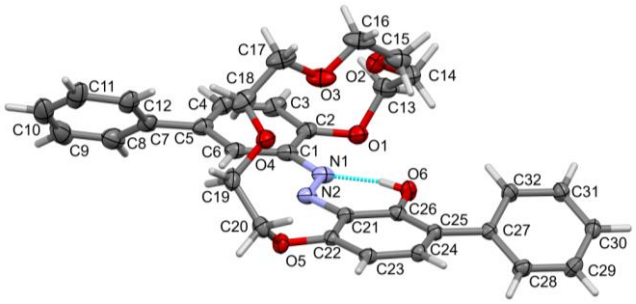

Figure 12. Molecular view of **Ph-19-*o*-OH** showing atom labelling scheme. Intramolecular hydrogen bonding drawn as the dashed cyan line. Disordered OH group shown only at C26. Displacement ellipsoids drawn at 50% probability level. Selected bond lengths (Å) and angles (°): O6-C26 1.3234(19), N1-N2 1.2761(16), C1-N1 1.4004(16), N2-C21 1.4104(15), C1-N1-N2 117.53(12), C21-N2-N1 113.41(11). For torsions in the linker ether see Table S7.

Crystal packing in all investigated structures, due to absence of classical intermolecular hydrogen bonding, is influenced mainly by stacking interactions (see Table S8). In the case of **Ph-19-*p*-OH(1)**, two molecules are wrapped around a local symmetry center with part of the ether linker placed between the rings of the second molecule. Stability of this pair is ensured by mutual stacking interaction of rings C1-C6 and C13-C18, see Figure S18. Due to the absence of symmetry centers in **Ph-19-*p*-OH(2)**, packing of molecules in the second polymorph is different. The two-symmetry independent molecule shows stacking interactions with their translation related equivalents with practically no penetration of the linker between the aromatic rings (Figure S19).
The stacks of molecules are then packed in an inclined way when looking along crystallographic c direction. Stacking interactions were also found in **Ph-20-ester**. Two molecules are gathered around a symmetry center, this time with linker loops directed outside the center of the molecular complex. The "dimers" are then stacked in the solid using mainly weaker van der Waals intermolecular interactions, see Figure S20. Crystal packing of **Ph-19-*o*-OH** is shown in Figure S21. Previously we have reported X-ray structures of ***t*-Bu-19-*o*-OH**, ***t*-Bu-20-ester** and ***t*-Bu-19-*p*-OH**.[38,39] Generally conformation of the polyether link in new structures resembles previous findings. The link goes over the azo group in both ***t*-Bu-19-*o*-OH** and **Ph-19-*o*-OH** (see Figure 12). It is almost flat in cases of ***t*-Bu-19-*p*-OH** and **Ph-19-*p*-OH** and tilted in half for both ***t*-Bu-20-ester** and **Ph-20-ester**.

Structure of Ph-17-*p*-OH and Ph-20-ester in solution

The structure of **Ph-17-*p*-OH** was determined by NMR methods, based on ROESY, gHSQC and gHMBC spectra (Figure 13 and Figure S5a-e).

The ROE effect of H-A3/H-B5 reflects the direct chemical bonding of rings A and B. Similar spatial relationships of rings A and C and B and D reflect ROEs H-A3/H-C2 and H-B5/H-D2.
The location of oligoether chain attachment sites is determined by ROEs H-1/H-A6 and H-8/H-B2. In the ^{13}C spectrum (Figure S5c), three signals (C-B1, C-A1, C-B3) are observed in the range characteristic for aromatic ethers/alcohols. Their identification was made based on the H/C couplings observed in the gHMBC spectrum, namely: H-1/C-A1, H-8/C-B1, H-B5/C-B1, H B5/C B3 and H-A5/C-A1, and H-A3/C-A1. Coupling series: H-C2/C-A4, H-A3/C-B6, H-B5/C-A2 and H-B5/C-D1 reflect the direct covalent bond connections of the C, A, B and D rings. The phenolic proton was revealed in the ^{1}H spectrum recorded in DMSO-d_6 at a shift of 9.8 ppm (Figure S5a).
A series of analogous NMR experiments were also performed for **Ph-20-ester**. The structure of the compound in solution, determined by NMR methods, is in full agreement with the results obtained from X-ray diffraction analysis (Figure 14 and Figure S4a-h).
In terms of spatial relationships, a consistent set of NOE effects observed in the ROESY spectrum was obtained (Figure S4e). Among many others, the most significant were: strong ROEs between H5'a, and H-g1, H-g2 and H-4, as well as ROEs H-g1/H-1, H-4/H-1". The absence of ROE H-g8/H-1' well reflects the increased distance between H-g8/H-1 as a result of the rearrangement of the aromatic ring with the formation of a C-6' carboxyl group in place of the original ether group.
The analysis of the carbon skeleton was based on the analysis of the H/C couplings observed in the gHSQC and gHMBC spectra (Figure S4g and Figure S4h). The list of the most significant correlations includes: H-g1/C-6, H-5'a/C-5,C-4,C-4', H-g8/C-6', H-1'/C-6', and H-4/C-6" and H-3'/C-6".

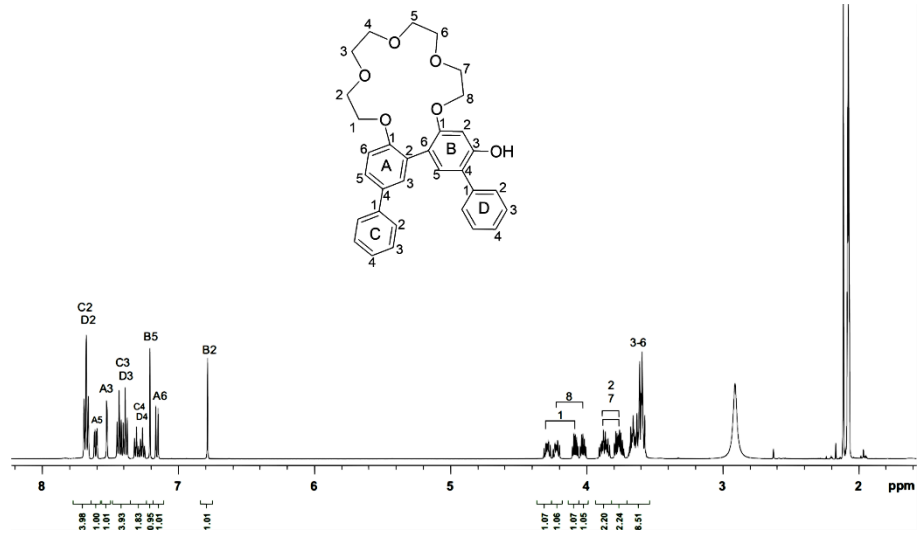

Figure 13. ^{1}H NMR spectrum of **Ph-17-*p*-OH** (acetone-d_6).

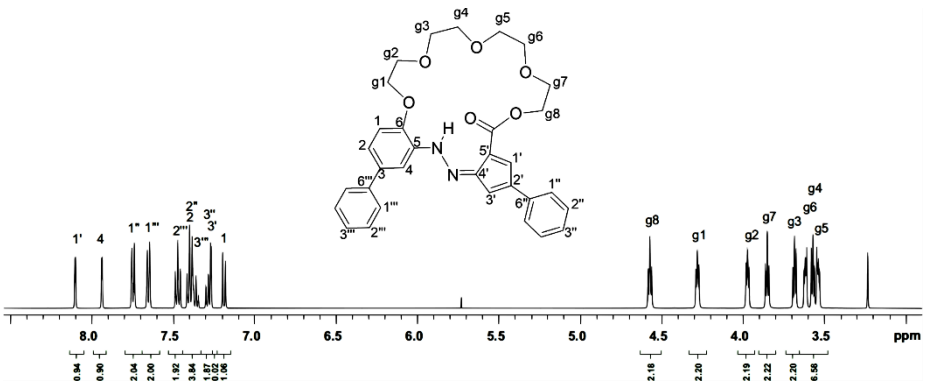

Figure 14. ^{1}H NMR spectrum of **Ph-20-ester** (DMSO-d_6).

Optical sensor layers – preliminary studies

Ph-19-*p*-OH chromoionophore was used in preliminary studies as a component of optical sensor layer by immobilizing it on a porous glass (PG) modified with polystyrene. Such prepared sensor layers were investigated as a material that changes its

color upon contact with aqueous solutions of metal salts. As metal cation complexation in acetonitrile was investigated for alkali and alkaline earth metal cations, the color change of **Ph-19-*p*-OH** upon its immobilization was investigated in the presence of nitrates of these metals first. Material was immersed in 0.1 M aqueous solutions of alkali and alkaline earth metal nitrates (of pH 6.3-6.8). After drying the material with hot air, a slight color change was observed: from yellow to bright yellow for potassium and strontium, with the most significant, however not spectacular, change from yellow to orange for magnesium (Figure 15). It was found that immersion in solution of lead(II) nitrate causes more noticeable, than in case of alkali and alkaline metal salts, color change of receptor layer: from yellow to bright yellow (Figure S22a). This, to some degree, can be an analogy to the complex formation with alkali and alkaline metal cations in solution (hypsochromic shift of absorption band is observed upon complex formation in acetonitrile) which corresponds to change of color of receptor layer upon contact with e.g. potassium or strontium salts (Figure 15).
From preliminary studies, the linear response range (given as ΔE_{RGB}) towards lead(II) is 10^{-2}-5$\cdot 10^{-5}$ M (R2=0.9788, Figure S22b) was estimated. However, the more promising seems to be the experiment, where the experiment, in which aluminum nitrate was used seems more promising. Upon contact with aqueous solution of this metal salt, the color of the sensing layer turned from yellow to pink (Figure S23). Taking into account that color response might be a result of pH of the aqueous solution of salt, additional experiments were done using nitric acid (Figure S24) solutions and aluminum nitrate solution of fixed pH (Figure 16). Estimated linear response range towards Al(III) (given as ΔE_{RGB}) towards lead(II) is $1\cdot 10^{-1}$-$1\cdot 10^{-4}$ M (R2=0.97755, Figure 16a) and $1\cdot 10^{-1}$-$5\cdot 10^{-5}$ M (R2=0.9785, Figure 16b) with LOD $4.85\cdot 10^{-4}$ M and $1.54\cdot 10^{-4}$ M for pH 3 and 4 respectively.

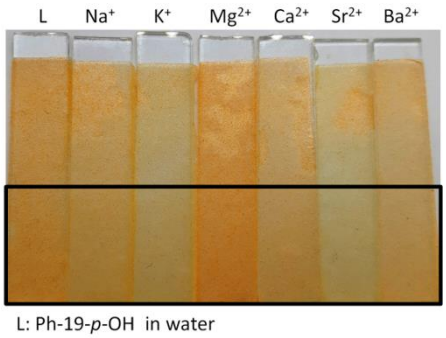

Figure 15. Change of color of optical sensing layers with **Ph-19-*p*-OH** as chromoionophore after immersion in 0.1 M solutions of alkaline and alkali earth metal nitrates (pH = 6.3 – 6.8); composition of optode: 0.85 mg **Ph-19-*p*-OH**/1g porous glass.

Preliminary results have shown, for the first time, the possibility of effective immobilization of *p*-hydroxyazobenzocrown in the receptor layer of the optical sensor. The assessment of the potential use of such prepared sensors obviously needs more detailed studies including the influence of the interfering ions, such as the effect of counter ion in salts. Such investigation is critical if the application of the sensors for determination of aluminum in real samples e.g. natural waters or biological fluids is considered. Aluminum is one of the most abundant metallic element used nowadays in food,[e.g. 53] drugs such as antacids,[54] or in water treatment as coagulant.[55] It was proved that excessive levels of this element might cause neurological diseases such as Alzheimer's disease[56] and also may affect bones' condition.[57,58] World Health Organization (WHO) has set a maximum contaminant level (MCL) of aluminum in drinking water as 7.4 μM.[59]
In our opinion, further studies on the applications of *p*-hydroxyazobenzocrowns as chromoionophores in metal cation sensing layers are promising and worth attention.

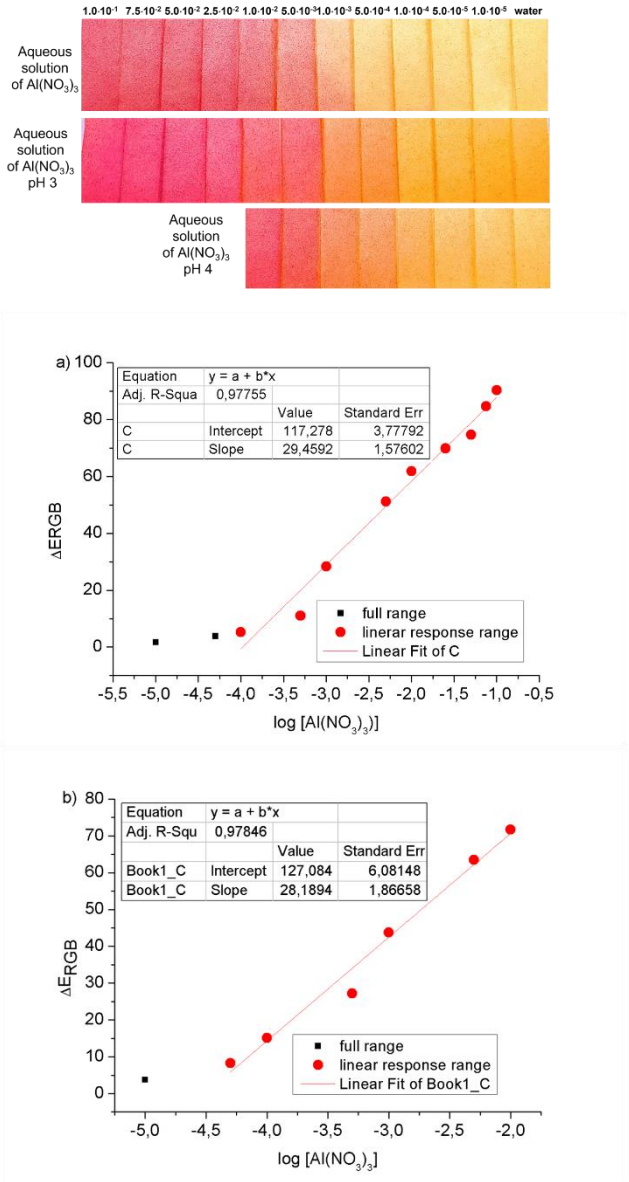

Figure 16. Top: Color change of the sensing layers based on PG with **Ph-19-*p*-OH** as chromoionophore in the presence of aqueous solutions of aluminum nitrate and aluminum nitrate at fixed pH: a) and b) colorimetric response of receptor layer - given as ΔE_{RGB} towards aluminum nitrate at pH 3 and 4 respectively.

Conclusions

Studies on the effect of the presence of additional substituents in benzene rings of azoxybenzocrowns on the products of their photo- and thermal rearrangement and on the properties of compounds obtained by this method were extended to derivatives with phenyl substituents. It was found that photo rearrangement of 19-membered azoxybenzocrowns leads mainly to formation of *para*- and *ortho*-hydroxyazobenzocrowns. The yield of this transformation depends on the presence and type of the substituents in benzene rings in *para* position to oligoether moiety. *Para*-hydroxyazobenzocrowns are preferentially formed (with comparable yields - over 50% - for all investigated derivatives) in propan-2-ol. *Ortho* isomer formation is favored in the acidified toluene as a solvent (over 70% yield). The highest yield (75%) of *ortho*-hydroxyazobenzocrown was found for sterically hindered macrocycle bearing *t*-butyl groups in acidified propan-2-ol. Under these conditions the transformation of unsubstituted and phenyl derivatives was below 40%. The effect of the substituents on photo- and thermal rearrangements of 19-membered azoxybenzocrowns is more interesting, when where atypical products of these processes - cyclic aldehydes and esters - are compared. The presence of substituents in *para* position in benzene rings seems to be a necessary condition for thermochemical rearrangements to occur.

The presence of substituents in benzene rings affects tautomeric equilibrium of 19-membered *p*-hydroxyazobenzocrowns in DMSO and acetonitrile solution. The contribution of azophenol tautomer is the highest in case of unsubstituted *p*-hydroxyazobenzocrown **19-*p*-OH** and lower in substituted ones. Bulky *t*-butyl groups affect tautomeric equilibrium stronger than flat phenyl moieties. Tautomeric equilibrium of 19-membered *o*-hydroxyazobenzocrowns is not affected by the presence of substituents - these compounds in solution exist in azophenol forms.
Metal cation affinity of *p*-hydroxyazobenzocrowns is connected with the presence of substituents in benzene rings. For alkali metal cation complexes with higher values of stability constants are observed for unsubstituted macrocycle, whereas alkaline earth metal cations are bound more strongly by substituted *p*-hydroxyazobenzocrowns.
The effect of the presence of substituents in benzene rings is well seen for *o*-hydroxyazobenzocrowns in case of formation of complexes with alkaline earth metal cations. While the differentiation in selectivity can be seen for unsubstituted macrocycle and its *t*-butyl bearing analog, for 19-membered macrocycle with phenyl residues the values of stability constants are more or less comparable. This can point to the influence of the substituents on the size and geometry of the molecular cavity which results in observed metal cation binding strength.
For the first time *p*-hydroxyazobenzocrowns were used as components of receptor layers of optical sensors. Even though the results presented here are preliminary in nature, it seems that not investigated, until now, in this regard macrocycles can be promising sensing molecules not only in solution, but also upon immobilization on solid matrix. X-ray structural analysis shows a large variety in conformation of the investigated molecules in crystalline state. The most striking difference in molecular conformation is the *trans* location of polyether linker ends in ring-N=N-ring moiety in **Ph-19-*o*-OH**, being *cis* in the **Ph-19-*p*-OH** molecules. This may be caused by formation of strong OH…N hydrogen bonding between hydroxy and diazo groups, which is not possible in *para*-OH substituted isomers. This is accompanied with tautomeric form change in the crystalline state: **Ph-19-*o*-OH** forms azophenol, while **Ph-19-*p*-OH** is quinone-hydrazone.
The effect of substituents in benzene rings on the properties of hydroxyazobenzocrowns is under further investigation in our group.

Experimental Section

Materials and methods

Unless otherwise stated, materials and solvents were of analytical reagent grade obtained from commercial suppliers and were used without further purification. UV-Vis and spectrofluorometric measurements were carried out in commercial solvents of the highest available purity: DMSO (spectroscopic-grade, POCh, Gliwice, Poland), dichloromethane (LiChrosolv and SupraSolv, MERCK, Darmstadt, Germany), methanol (HPLC grade, POCh, Gliwice, Poland) and acetonitrile (LiChrosolv, MERCK, Germany). For measurements performed in mixed, water-containing systems, deionized water (conductivity <1 $\mu S \cdot cm^{-1}$, Hydrolab, Straszyn, Poland) was used.
Photochemical reactions were carried out in quartz flasks using a photoreactor prototype designed by Dariusz Wysiecki MSc., Eng. and constructed in cooperation with the Enviklim Company (Gdańsk, Poland). The reactor is equipped with 3 UVA diode arrays (2 × UV-D6565-4LED, 40 W and 1 × UV-D6565-15LED, 150 W, λ = 365–370 nm).[38,39] ^{1}H and ^{13}C NMR spectra were recorded on a Varian INOVA 500 spectrometer at 500 and at 125 MHz, respectively. Chemical shifts are reported in δ (ppm) units. FTIR spectra (film) were taken on Nicolet iS10 apparatus. High resolution mass spectra (HRMS) were taken on a SYNAPT G2-S HDMS (Waters) spectrometer with electrospray ionization source (ESI) and a TOF mass analyzer. UV-Vis measurements were carried out with the use of UNICAM UV 300 series spectrometer. Fluorescence spectra were recorded on a luminescence spectrometer (AMINCO Bowman Series 2 spectrofluorimeter) using the flash xenon lamp. The bandpass of excitation and emission monochromators was 16 nm. UV-Vis and fluorescence measurements were carried out in 1 cm quartz cuvettes.

Preparation

The reaction progress and purity of products were monitored by TLC using aluminum sheets covered with silica gel $60F_{254}$ (Merck). UV light (254 nm) was used as the detection method. Reaction mixtures were separated using a classical column (silica gel 60, 0.063-0.200 mm, Merck) or preparative thin layer (PTLC plates, silica gel $60F_{254}$, 1mm, 20□20 cm size, Merck) chromatography. Reagent grade solvents were used.

Preparation - experimental details

Preparation of substrate for rearrangements – di-phenyl-19-azoxybenzocrown (**Ph-19-Azo-O**). This compound was prepared first time by Skwierawska and others.[60]
Ph-19-Azo-O was prepared according to optimized by us protocol, analogously to the 19-membered di-*tert*-butylazoxybenzocrown.[39] Starting from 11.0 g of 1,11-bis(2-nitro-4-phenylphenoxy)-3,6,9-trioxaundecane (podand), 4.6 g (46%) of phenyl-19-azoxybenzocrown (**Ph-19-Azo-O**) as white solid was obtained. Mp 142-143 □C (with rearrangement, change of color of liquid to red). The substance was stored in the absence of light.

^{1}H NMR (acetone-d_6, 500 MHz), δ: 8.33 (1H, d, J=2.2 Hz), 8.06 (1H, d, J=2.5 Hz),7.84 (1H, dd, J1=8.5 Hz, J2=2.5 Hz), 7.74 (2H, d, J=7.4 Hz), 7.68 (2H, d, J=7.2 Hz), 7.66 (1H, dd, J1~8.5 Hz, J2=2.2 Hz), 7.51 (2H, d, J=7.4 Hz), 7.47 (2H, d, J=7.4 Hz), 7.43 (1H, d, J=8.8 Hz), 7.41-7.35 (2H, m), 7.29 (1H, d, J=8.5 Hz), 4.39 (2H, t, J=5.2 Hz), 4.32 (2H, t, J=5.2 Hz), 3.93 (1H, t, J=5.2 Hz), 3.91 (2H, t, J=5.2 Hz), 3.66-3.63 (4H, m), 3.57-3.59 (4H, m). ^{13}C NMR (acetone-d_6, 125 MHz), δ: 152.6, 150.6, 140.7, 140.2, 138.0, 134.6, 133.6, 133.0, 129.1, 129.0, 128.9, 127.5, 127.4, 126.9, 126.6, 125.5, 123.2, 121.3, 115.5, 114.0, 71.1, 70.9, 70.6, 70.6, 69.3, 69.3, 69.2, 68.6. FT-IR (film, cm^{-1}) $\tilde{\nu}$ = 3057, 3032, 2922, 2874, 1615, 1600, 1517, 1487, 1460, 1450, 1276, 1140, 954, 762, 699, 607. TLC: R_{f1}=0.35 (chloroform:methanol, 30:1), R_{f2}=0.38 (dichloromethane:acetone, 5:1, v/v).

Photochemical rearrangement of Ph-19-Azo-O

Ph-19-Azo-O in a 150 mL quartz Erlenmeyer flask (typically 60–78 mg, input details in Table 2, *vide infra*) dissolved in the given
solvent (130 mL per 70 mg of substrate) was subjected to UV irradiation for approx. 75 min in the photoreactor. Within the timescale of the experiment the temperature of the solution increased up to ~70-75 °C. As a result of the reaction progress the color of the solution changed from light yellow to red-orange. After that time the mixture was quantitatively transferred to a round bottom flask to evaporate the solvent under reduced pressure. After dissolution in dichloromethane products of the photochemical rearrangement were isolated by preparative thin layer chromatography with a dichloromethane:acetone mixture (10 : 1, v/v) as the mobile phase. (Additional PTLC isolation of **19-al** from the mixture with **19-*o*-OH** in CH_2Cl_2:acetone (10 : 1) was conducted). The separated products were eluted from silica gel with a mixture of chloroform-methanol. After filtration and solvent evaporation, the residue was dissolved in dichloromethane and filtrated one more time. Then the solvent was evaporated and the residue was weighed. Samples of isolated **Ph-17-*p*-OH,** if containing unreacted azoxy compound, were purified by PTLC using mixture chloroform:methanol (30:1 , v/v) as an eluent.
Yields of photochemical rearrangement products: **Ph-20-ester**, **Ph-19-*o*-OH**, **Ph-17-*p*-OH**, **Ph-19-*p*-OH** and **Ph-19-al** are collected in Table 2.

Table 2. Inputs and yields of macrocyclic products obtained in photochemical rearrangements of **Ph-19-Azo-O**.

Solvent	Input: **Ph-19-Azo-O** [mg]	Yield [mg], (yield) [%]					**Ph-19-Azo-O** recovery [mg] ([%])	Overall yield of isolated products of rearrangement [%]
		Ph-20-ester [mg] ([%])	**Ph-19-*o*-OH** [mg] ([%])	**Ph-19-al** [mg] ([%])	**Ph-17-*p*-OH** [mg] ([%])	**Ph-19-*p*-OH** [mg] ([%])		
toluene	77.6	6.5 (8.4)	22.4 (28.9)	11.0 (14.2)	10.7 (13.8)	4.0 (5.2)	22.9 (29.5)	70.5
toluene[a]	126.7	8.6 (6.8)	36.4 (28.7)	17.5 (13.8)	17.6 (13.9)	6.8 (5.4)	39.8 (31.4)	68.6
toluene/acetic acid[b]	77.4	—	53.8 (69.5)	—	5.5 (7.1)	3.1 (4.0)	15.0 (19.4)	80.6
2-propanol	59.7[c]	0.8 (1.4)	6.2 (10.3)	0.7 (1.2)	4.2 (7.1)	31.6 (53.0)	16.1 (27.0)	73.0
2-propanol/ acetic acid[b]	60.0[c]	0.4 (0.7)	20.2 (33.6)	1.8 (3.0)	2.0 (3.3)	6.9 (11.5)	28.7 (47.9)	52.1

[a] 255 mL; [b] acetic acid 0.2 mL [c] inputs in propan-2-ol are due to lower solubility of substrate in this solvent

Thermochemical rearrangement of Ph-19-Azo-O

Two thermochemical reactions were performed to determine the effect of temperature on the conversion of a 19-membered azoxybenzocrown **Ph-19-Azo-O**.
48 mg of **Ph-19-Azo-O** in a round bottom flask was placed in an oil bath of temperature 156-158°C. The content of the flask was heated for 2 hours in the dark. The white, cottony substrate, after heating, changed its form to a hard, dark cherry-colored substance, which, had a blood-red color when dissolved in dichloromethane. TLC chromatography of the resulting solution was performed in the system chloroform:methanol (30 : 1, v/v). TLC plate showed a single spot pointing out one major product of the thermal process. The resulting compound was purified and isolated by column chromatography, where silica gel was suspended in dichloromethane and dichloromethane:acetone 20:1 was used as the mobile phase. The product was identified as **Ph-20-ester**. Thermal conversion yields 88%.
For comparison, an experiment with 23.9 mg of **Ph-19-Azo-O** dissolved in 10 ml of toluene heated in an oil bath at 75°C for 80 min was also performed. The light-yellow solution did not change appearance after heating in the dark. The TLC control plate (chloroform:methanol, 30:1 v/v) showed a single spot corresponding to an unreacted substrate **Ph-19-Azo-O**.

Spectral characterization of products of photochemical and thermochemical rearrangements of Ph-19-Azo-O.

For obtained and studied here functionalized azocompounds no *cis*⇄*trans* isomerization was found to occur.

Ph-19-p-OH
Obtained as an orange solid, mp 159-160 □C.
^{1}H NMR (DMSO-d_6, 500 MHz), signals for dominating azophenol form are given δ: 10.43 (1H, s), 7.70 (1H, dd, *J1*=8.5 Hz, *J2*=2.1 Hz), 7.66 (2H, d, *J*=7.3 Hz), 7.55 (2H, d, *J*=7.3 Hz), 7.26-7.46 (8H, m), 7.23 (1H, s), 6.75 (1H, s), 4.26-4.54 (4H, m), 3.69-3.78 (4H, m), 3.44-3.52 (4H, m), ca. 3.3-3.4 (4H, under water signal). ^{13}C NMR (DMSO-d_6, 125 MHz), δ: 158.7, 155.6, 152.7, 145.6, 139.6, 138.0, 138.0, 132.9, 129.4, 129.4, 128.5, 128.3, 127.5, 127.0, 126.7, 121.1, 120.8, 117.7, 114.9, 101.8, 70.5, 70.5, 70.4, 68.8, 68.7, 68.6. HRMS (ESI) m/z: $[M+Na]^+$ calc. for $C_{32}H_{32}N_2O_6Na$ 563.2158; found 563.2162. FTIR (film, cm^{-1}): ν̃ = 3312, 3054, 2926, 1625, 1593, 1506, 1449, 1421, 1351, 1266, 1205, 1178, 1125, 1056, 940, 865, 762, 734, 698.
TLC: R_{f1} = 0.21 (chloroform:methanol, 30:1), R_{f2} = 0.06 (methylene chloride acetone, 10:1).

Ph-19-o-OH
Obtained as dark brown solid, mp 163-165 °C.
^{1}H NMR (DMSO-d_6, 500 MHz): δ 14.55 (1H, s), 7.84 (1H, d, *J*=2.2 Hz), 7.80 (dd, 1H, *J1*=8.5 Hz, *J2*=2.2 Hz), 7.68-7.72 (2H, m), 7.58-7.61 (2H, m), 7.42-7.52 (6H, m), 7.39 (1H, t, *J*=9 Hz), 7.34 (1H, t, *J*=9 Hz), 6.83 (1H, d, *J*=8.8 Hz), 4.40-4.42 (4H, m), 3.73-3.75 (2H, m), 3.65-3.67 (2H, m), 3.42 (2H, t, *J*=4.3 Hz); 3.31 (2H, t, *J*=4 Hz), 3.16-3.20 (4H, m).
^{13}C NMR (DMSO-d_6, 125 MHz): δ 158.4, 154.7, 152.3, 141.9, 139.6, 137.5, 135.7, 134.3, 130.5, 130.4, 129.5, 129.5, 128.6, 127.9, 127.2, 126.9, 123.3, 118.6, 116.5, 107.0, 71.3, 71.2, 70.6, 70.2, 70.0, 70.0, 69.9, 69.7. HRMS (ESI) *m/z*: $[M+Na]^+$ calc for: $C_{32}H_{32}N_2O_6Na$ 563.2158; found 563.2159. FTIR (film, cm^{-1}): ν̃ = 3422, 3057, 3032, 2922, 2868, 1602, 1483, 1288, 1268, 1227, 1132, 1101, 759, 698.
TLC: R_{f1} = 0.42 (chloroform:methanol, 30:1), R_{f2} = 0.32 (methylene chloride:acetone, 10:1).

Ph-19-al
Obtained as a brown solid, mp 206-208 °C.
^{1}H NMR (DMSO-d_6, 500 MHz), δ: 11.36 (1H, s), 9.78 (1H, s), 7.72 (1H, d, *J*=2.2 Hz), 7.63 (2H, d, *J*=7Hz), 7.58 (2H, d, *J*=7 Hz), 7.46-7.52 (5H, m), 7.41 (1H, dd, *J1*=7.0 Hz, *J2*=2.0 Hz), 7.36 (1H, t, *J*=7.0 Hz), 7.25 (1H, d, *J*=8.5 Hz), 6.12 (1H, s), 4.28-4.35 (4H, m), 3.02-3.98 (4H, m), 3.60-3.70 (8H, m). ^{13}C NMR (DMSO-d_6, 125 MHz), δ: 187.2, 148.4, 146.2, 139.8, 138.0, 133.9, 133.8, 132.1, 129.5, 128.7, 128.4, 127.7, 126.5, 123.2, 113.8, 112.4, 98.9, 71.3, 71.2, 71.1, 70.6, 70.6, 69.3, 68.9, 68.8. HRMS (ESI) m/z: calc. for $C_{32}H_{32}N_2O_6Na$ $[M+Na]^+$ 563.2158; found 563.2167. FTIR (film, cm^{-1}): ν̃ = 3299, 2921, 1644, 1552, 1525, 1482, 1396, 1371, 1264, 1148, 884.
TLC: R_{f1} = 0.57 (chloroform:methanol, 30:1), R_{f2} = 0.43 (methylene chloride:acetone, 10:1).

Ph-20-ester
Obtained as a dark red solid, mp 150-151 °C.
^{1}H NMR (DMSO-d_6, 500 MHz), δ: 14.26 (1H, s), 8.15 (1H, s), 7.94 (1H, s), 7.79 (2H, d, *J*=7.5 Hz), 7.61 (2H, d, *J*=7.5 Hz), 7.49 (2H, t, *J*=7.5 Hz), 7.21-7.44 (7H, m), 4.56-4.61 (2H, m), 4.28-4.34 (2H, m), 3.95-4.02 (2H, m), 3.83-3.89 (2H, m), 3.50-3.62 (8H, m). ^{13}C NMR (DMSO-d_6, 125 MHz), δ: 166.0, 147.4, 144.1, 142.0, 140.1, 138.1, 134.3, 134.2, 132.3, 129.4, 129.4, 128.0, 127.7, 127.0, 126.9, 125.6, 123.7, 115.7, 113.8, 112.7, 71.0, 70.9, 70.8, 70.6, 69.5, 69.0, 64.6. HRMS (ESI) m/z: calc. for $C_{32}H_{32}N_2O_6Na$ $[M+Na]^+$ 563.2158 found 563.2164. FTIR (film, cm^{-1}): ν̃ =2923, 1670, 1664, 1554, 1459, 1448, 1279, 1247, 1208, 1125, 1080, 759.
TLC: R_{f1} = 0.67 (chloroform:methanol, 30:1), R_{f2} = 0.44 (methylene chloride:acetone, 10:1).

Ph-17-p-OH
Obtained as a colorless solid, mp 169-171 °C.

^{1}H NMR (DMSO-d_6, 500 MHz), δ: ca. 8-9 ppm (broad and weak signal; observable in amplification mode), 7.68 (4H, t, *J*=7 Hz), 7.60 (1H, dd, *J1*=8.7 Hz, *J2*=2.5 Hz), 7.52 (1H, d, *J*=2.5 Hz), 7.44 (2H, t, *J*=7.7 Hz), 7.38 (2H, t, *J*=7.8 Hz), 7.31 (1H, t, *J*=7.3 Hz), 7.26 (1H, t, *J*=7.3 Hz), 7.21 (1H, s), 7.15 (1H, d, *J*=8.3 Hz), 6.79 (1H, s), 4.26-4.31 (1H, m), 4.20-4.25 (1H, m), 4.06-4.10 (1H, m), 4.02-4.05 (1H, m), 3.82-3.91 (2H, m), 3.72-3.80 (2H, m), 3.57-3.68 (8H, m). ^{13}C NMR (aceton-d_6, 125 MHz), δ: 157.0, 156.7, 154.6, 140.7, 138.7, 132.9, 132.8, 129.9, 129.2, 129.0, 128.7, 127.9, 126.5, 126.4, 126.0, 120.5, 120.2, 112.2, 100.5, 70.9, 70.8, 70.4, 70.4, 69.35, 69.2, 67.7, 67.7, 54.1. HRMS (ESI) m/z: calc. for: $C_{32}H_{32}O_6Na$ $[M+Na]^+$ 535.2097; found 535.2098. FTIR (film, cm^{-1}): $\tilde{\nu}$ = 3249, 3057, 3028, 2923, 2869, 1610, 1482, 1406, 1274, 1265, 1248, 1179, 1128, 1061, 764, 699.
TLC: R_{f1} = 0.38 (chloroform:methanol, 20:1), R_{f2} = 0.13 (methylene chloride:acetone, 10:1).
UV-Vis spectral characterization of products of the rearrangements are collected in Table 3.

Table 3. The position of absorption bands λ [nm] and values of molar absorption coefficient **ε** [$dm^3 \cdot mol^{-1} \cdot cm^{-1}$] in UV -Vis absorption spectra in acetonitrile for products of rearrangements.

Compound	λ [nm]	ε [$dm^3 \cdot mol^{-1} \cdot cm^{-1}$]
Ph-19-*p*-OH	453	2.87×10^4
Ph-19-*o*-OH	344	1.57×10^4
Ph-19-al	440	2.43×10^4
Ph-20-ester	443 504	1.58×10^4 1.97×10^4
Ph-17-*p*-OH	204 256	1.80×10^3 1.22×10^3
Ph-19-Azo-O	258	4.15×10^4

X-ray Crystal Structure Determination

Diffraction intensity data for **Ph-19-*p*-OH(1)**, **Ph-19-*p*-OH(2)** and **Ph-20-ester** were collected on an IPDS 2T dual beam diffractometer (STOE & Cie GmbH, Darmstadt, Germany) at 120.0(2) K with CuK□ radiation of a microfocus X-ray source (GeniX 3D Cu High Flux, Xenocs, Sassenage, 50 kV, 0.6 mA, and λ = 1.54186 Å). Data for **Ph-19-*o*-OH** were collected using MoK□ radiation of a microfocus X-ray source (GeniX 3D Mo High Flux, Xenocs, Sassenage, 50 kV, 1.0 mA, and λ = 0.71073 Å). Investigated crystals were thermostated under a nitrogen stream at 120 K using the CryoStream-800 device (Oxford CryoSystem, UK) during the entire experiment.
Data collection and data reduction were controlled by using the X-Area 1.75 program (STOE, 2015). Absorption correction was performed by integration method or by multi-scan method, no correction was applied for **Ph-19-*o*-OH** due to low μ coefficient. The structure was solved using intrinsic phasing implemented in SHELXT and refined anisotropically using the program packages Olex2[61] and SHELX-2015.[62,63] Positions of the C–H hydrogen atoms were calculated geometrically taking into account isotropic temperature factors. All hydrocarbonic H-atoms were refined as riding on their parent atoms with the usual restraints. NH atoms were found in the Fourier electron density map and refined with N-H distance constrained to 0.88(2) Å for all molecules.
Structure **Ph-19-*p*-OH(1)** was refined with no special treatment. Structure of **Ph-20-ester** was refined using additionally the squeeze procedure for removing electron density of disordered solvent molecules (methanol + water). Structure of **Ph-19-*o*-OH** was refined with the one OH group disordered over two positions (substituted at C6 or at C26 atom), at two rings which induced disorder of the related H atoms. Site occupation factors attribute 54.1% of OH group at C26 and 45.9% at C6.
Crystal data and structure refinement details for **Ph-19-*p*-OH**(1), **Ph-19-*p*-OH**(2), **Ph-20-ester** and **Ph-19-*o*-OH** are listed in Table S9. Crystallographic data for all structures reported in this paper have been deposited with the Cambridge Crystallographic Data Centre as supplementary publication No. CCDC 2192740, 2192741, 2192742 and 2192743 for **Ph-19-*p*-OH(1)**, **Ph-19-*p*-OH(2)**, **Ph-20-ester** and **Ph-19-*o*-OH** respectively. Deposition Number(s) 2192740 (for **Ph-19-*p*-OH(1)**), 2192741 (for **Ph-19-*p*-OH(2)**), 2192742 (for **Ph-20-ester**), 2192743 (for **Ph-19-*o*-OH**) contain(s) the supplementary crystallographic data for this paper. These data are provided free of charge by the joint Cambridge Crystallographic Data Centre and Fachinformationszentrum Karlsruhe Access Structures service.

Complexation studies

For metal cation complexation, lithium perchlorate (99.9%, Sigma Aldrich, Milwaukee, WI, USA), sodium perchlorate monohydrate (>99%, Fluka, Buchs, Switzerland), potassium perchlorate (>99%, Sigma Aldrich, Milwaukee, WI, USA), magnesium perchlorate (≤100%, Sigma Aldrich, Steinhaim, Germany), calcium perchlorate tetrahydrate (99%, Sigma Aldrich, Milwaukee, WI, USA), strontium perchlorate trihydrate (≤100%, Sigma Aldrich, Steinhaim, Germany), barium perchlorate (97%, Sigma Aldrich, Steinhaim, Germany) were used. For acid-base properties studies *p*-toluenesulfonic acid monohydrate (pure, POCH, Gliwice, Poland), *tetra-n*-butylammonium hydroxide 30-hydrate (98%, Sigma-Aldrich, Steinhaim, Germany) were used. Complexation studies were performed by spectrophotometric titration of the crown solution in acetonitrile with the respective metal perchlorate (for metal cations). The stock solutions of azobenzocrowns (~10^{-4} M), metal perchlorates (~10^{-2} M), *p*-toluenesulfonic acid (~10^{-2} M) and *tetra-n*-butylammonium hydroxide (~10^{-2} M) were prepared by weighing their respective quantities and dissolving in acetonitrile in volumetric flasks. For titrations, azobenzocrown solutions of 2.3 mL

starting volume in the cuvette were used. The stability constant values from titration experiments were calculated with the use of the OPIUM[66] program.
For evaluation of binding constant K from fluorescence measurements, where quenching of fluorescence was observed the following equation (1) was applied:

$$F_0/(F - F_0) = [a/(b - a)][1/K[M] + 1] \quad (1)$$

The stability constant was determined as the intercept (b)/slope (a) ratio from the plot $F_0/(F\text{-}F_0)$ versus $[M]^{-1}$. F_0 is the fluorescence intensity of hydroxyazobenzocrown, F - the fluorescence intensity in the presence of metal perchlorate, [M] - salt concentration.
Stern-Volmer constants K_{sv}[67] were determined graphically according to equation (2):

$$F_0/F = 1 + K_{SV}[Q] \quad (2)$$

where F_0 is the fluorescence intensity in the absence of quencher, F – fluorescence intensity in the presence of quencher, [Q] - quencher (metal perchlorate) concentration [M].

Quantum yield determination

Fluorescence quantum yield was determined according to literature procedure.[68] As a standard, fluoresceine (= 0.95)[69] solution in 0.1 M NaOH was used.
Determination of the fluorescence quantum yield ( ) of **Ph-19-*p*-OH** consisted of the following steps: (i) registration of absorption spectra of hydroxyazobenzocrown (acetonitrile) and standard solutions of concentrations of absorbance below 0.2, (ii) registration of emission spectra of hydroxyazobenzocrown and standard solutions (instrument settings, excitation wavelength λ_{ex} and emission wavelength λ_{em} the same for the standard and sample: λ_{ex} 434 nm, λ_{em} 536 nm, (iii) calculation of quantum yield using formula (3):

$$\Phi_x = (\frac{a_x}{a_s}) \cdot (\frac{n_x}{n_s})^2 \cdot \Phi_s \ (3)$$

where - fluorescence quantum yield, x - sample, s - standard, a - gradient of the plot of integrated fluorescence intensity against absorbance, n - refractive index of the solvent.

Ion recognition studies – sensing layer

Porous glass modified with polystyrene (PG-PS) (particle size 0.075-0.125 mm, Mw ~ 120000 Corning) was used as solid support. For studies of ion recognition studies aqueous solutions of nitric acid and following salt were used: $NaNO_3$ (≥99.8%), KNO_3 (≥99.8%), $Mg(NO_3)_2{\times}6H_2O$ (≥99.0%), $Ca(NO_3)_2{\times}4H_2O$ (≥99.0%), $Ni(NO_3)_2{\times}6H_2O$ (≥98.0%), $Zn(NO_3)_2{\times}6H_2O$ (≥98.0%), $Cd(NO_3)_2{\times}4H_2O$ (≥98.0%) and rest from POCH and $Cu(NO_3)_2{\times}3H_2O$ (≥99.5%) from Merck, $Pb(NO_3)_2$ (≥99.0%, Alfa Aesar, Massachusetts, USA). All aqueous solutions were prepared using ultra-pure water obtained by reverse osmosis (RO) from Hydrolab Poland station (conductivity <1 $\mu S \cdot cm^{-1}$).
The pH of solutions was measured by a pH-meter CPC-511 with glass electrode EPS-1 (ELMETRON), standardized with buffer solutions. Portable LED light box (23 × 23 × 23 cm) was used to guarantee the reproducibility of the photos (PULUZ, Photography Light Box, Shenzhen Puluz Technology Limited). Pictures were taken with a Smartphone Samsung Galaxy A8 Plus.

Preparation of sensing layer

Sensing layer was prepared by procedure elaborated in our group by Wagner-Wysiecka et.al.[70] 1g of porous glass modified with polystyrene (PG-PS) was treated with 3 ml of a of **Ph-19-*p*-OH** ($5.25{\times}10^{-4}$ M in acetonitrile). After evaporation of the solvent a yellow powder was obtained. Dry yellow material with the adsorbed chromoionophore was immobilized on the surface of 0.9 x 4.5 cm glass plates using a double-sided rubber tape.

Digital color analysis

Pictures (photos done with Samsung Galaxy A8 Plus Smartphone camera) were analyzed using free software ImageJ.[71,72] Color change of sensing layer given as ΔERGB[73,74] was calculated using equation (4):

$$\Delta E_{RGB} = [(R_0 - R)^2 + (G_0 - G)^2 + (B_0 - B)^2]^{1/2} \ (4)$$

where R0, G0 and B0 values correspond to the color of the sensor layer in the absence of metal salt (nitric acid), and R, G and B values correspond to the color of the sensor upon contact with the analyte solution. Limit of detection (LOD) was calculated according to relationship (5):

$$LOD = (3\sigma\text{-}b)/a \ (5)$$

where σ is the standard deviation of the blank, a is the slope and b is the intercept of the linear function ERGB = f(molar concentration of analyte).

Supporting Information

The data that support the findings of this study are available in the Supplementary Information of this article.

Acknowledgments

This work was supported by the Faculty of Chemistry, Gdańsk University of Technology, No. 035376 and 036276 —internal grants from statutory funds. The financial support to maintenance of research facilities used in these studies from Gdańsk University of Technology by the DEC--2/2021/IDUB/V.6/Si grant under the SILICIUM SUPPORTING CORE R&D FACILITIES – "Excellence Initiative - Research University" program is gratefully acknowledged. Joanna Woszczyk M.Sc. (Nuclear Magnetic Resonance Laboratory, Gdańsk University of Technology, Faculty of Chemistry) is kindly acknowledged for her engagement and registering most of NMR spectra.

Conflict of Interest

The authors declare no conflict of interest.

Data Availability Statement

The data that support the findings of this study are available from the corresponding author upon reasonable request.

Keywords: azobenzocrown, azoxymacrocycle, photorearrangement, tautomerism, thermochemistry

[1] J. W. Steed, J. L. Atwood, in *Supramolecular Chemistry, 3rd Edition* (Ed. J. W. Steed, J. L. Atwood), John Wiley & Sons Ltd, **2022.**
[2] W. Y. Yi, F. L. Supian, M. Musa, N. F. N. Abd Karim, A. F. Naim, *Macromol. Res.* **2022**, *30*, 853-862.
[3] A. Cid-Samamed, J. Rakmai, J. C. Mejuto, J. Simal-Gandara, G. Astray, *Food Chem.* **2022**, *384*, 132467.
[4] A. Isik, M. Oguz, A. Kocak, M. Yilmaz, *J. Incl. Phenom. Macrocycl. Chem.* **2022**, *102*, 439-449.
[5] B. Xie, Y. F. Ding, M. Shiu, L. Yue, Ch. Gao, I. W. Wyman, R. Wang, *Eur. J. Nucl. Med. Mol. Imaging.* **2022**, *49*, 1200-1210.
[6] W. Li, W. Xu, S. Zhang, J. Li, J. Zhou, D. Tian, J. Cheng, H. Li, *J. Agric. Food Chem.* **2022**, *70*, 12746-12759.
[7] K. Vinod, H. Kim, B. Pandey, T. D. James, J. Yoon, E. V. Anslyn, *Chem. Soc. Rev.* **2023**, *52*, 663-704.
[8] A. Jain, A. Calò, D. Barceló, M. Kumar, *Anal. Bioanal. Chem.* **2022**, *414*, 5105-5119.
[9] G. Fukuhara, *J. Photochem. Photobiol. C* **2020**, *42*, e100340.
[10] R. Berkecz, G. Németi, A. Péter, I. Ilisz, *Molecules* **2021**, *26*, e4648.
[11] R. Berkecz, D. Tanács, A. Péter, I. Ilisz, *Molecules* **2021**, *26*, e3380.
[12] J. Ma, Y. Zhang, B. Zhao, Q. Jia, *Anal. Chim. Acta* **2020**, *1122*, 97-113.
[13] É. V. d'Astous, P. Dauphin-Ducharme, *Curr. Opin. Electrochem.* **2022**, *34*, 101029.
[14] Y. Y. Zhao, J. M. Yang, X. Y. Jin, H. Cong, Q. M. Ge, M. Liu, Z. Tao, *Curr. Org. Chem.* **2020**, *24*, 265-290.
[15] T. Rasheed, F. Nabeel, K. Rizwan, M. Bilal, T. Hussain, S. A. Shehzad, *TrAC - Trends Anal. Chem.* **2020**, *129*, e115958.
[16] C. Jiang, Z. Song, L. Yu, S. Ye, H. He, *TrAC - Trends Anal. Chem.* **2020**, *133*, e116086.
[17] Y. Sasaki, X. Lyu, W. Tang, H. Wu, T. Minami, *J. Photochem. Photobiol. C* **2022**, *51*, e100475.
[18] M. Mansha, S. A. Khan, Md. A. Aziz, A. Z. Khan, S. Ali, M. Khan, *Chem. Record* **2022**, *22*, e202200059.
[19] T. Minami, *Bull. Chem. Soc. Jpn.* **2020**, *94*, 24-33.
[20] E. Hosgor, A. Akdag, *Chem. Papers* **2022**, *76*, 3891-3898.
[21] X. Chi., W. Cen, J. A. Queenan, L. Long, V. M. Lynch, N. M. Khashab, J. L. Sessler, *J. Am. Chem. Soc.* **2019**, *141*, 6468-6472.
[22] E. Wagner-Wysiecka, N. Łukasik, J. F. Biernat, E. Luboch, *J. Incl. Phenom. Macrocycl. Chem.* **2018**, *90*, 189-257.
[23] P. Kumar, D. Gupta, S. Grewal, A. Srivastava, A. Kumar Gaur, S. Venkataramani, *Chem. Record* **2022**, *22*, e202200074.
[24] A. Blasceanu, M. Koerstz, A. B. Skov, K. V. Mikkelsen, M. B. Nielsen, *Angew. Chem. Int. Ed.* **2018**, *57*, 6069-6072.
[25] M. Shiga, H. Nakamura, M. Takagi, K. Ueno, *Bull. Chem. Soc. Jpn.* **1984**, *57*, 412-415.
[26] R. Tahara, T. Morozumi, H. Nakamura, M. Shimomura, *J. Phys. Chem. B.* **1997**, *101*, 7736-7743..
[27] E. Luboch, E. Wagner-Wysiecka, Z. Poleska-Muchlado, V. Ch. Kravtsov, *Tetrahedron* **2005**, *61*, 10738-10747.
[28] E. Wagner-Wysiecka, T. Rzymowski, M. Szarmach, M. S. Fonari, E. Luboch, *Sens. Actuat. B. Chem.* **2013,** *177*, 913-923.
[29] J. F. Biernat, E. Luboch, A. Cygan, *J. Coord. Chem.* **1992**, *27*, 215-217.
[30] Y. A. Simonov, E. Luboch, J. F. Biernat, N. V. Bolotina, V. E. Zavodnik, *J. Incl. Phenom. Macrocycl. Chem.* **1997**, *28*, 17-32.
[31] A. Skwierawska, E. Luboch, J. F. Biernat, V. Ch. Kravtsov, Y. A. Simonov, A. A. Dvorkin, V. K. Bel'skii, *J. Incl. Phenom. Macrocycl. Chem.* **1998**, *31*, 71-86 .
[32] E. Luboch, J. F. Biernat, V. C. Kravtsov, Y. A. Simonov, *J. Incl. Phenom. Macrocycl. Chem.* **1998**, *31*, 109-118.
[33] E. Luboch, J. F. Biernat, Y. A. Simonov, V. K. Bel'skii, *J. Incl. Phenom. Macrocycl. Chem.* **1999**, *11*, 109-118.
[34] O. Wallach, L. Belli, *Ber. Dtsch. Chem. Ges.* **1880**, *13*, 525-527.
[35] E. Luboch, *Pol. J. Chem.* **2008**, *82*, 1315-1318.
[36] G. M. Badger, R. G. Buttery, *J. Chem. Soc.* **1953**, 2156-2158.
[37] M. M. Shemyakin, T. E. Agadzhanyan, V. I. Maimind, R. V. Kudryavtsev, *Russ. Chem. Bull.* **1963**, *12*, 1216-1219.
[38] E. Wagner-Wysiecka, P. Szulc, E. Luboch, J. Chojnacki, K. Szwarc-Karabyka, N. Łukasik, M. Murawski, M. Kosno, *ChemPlusChem* **2020**, *85*, 2067-2083.
[39] E. Wagner-Wysiecka, P. Szulc, E. Luboch, J. Chojnacki, P. Sowiński, K. Szwarc-Karabyka, *Molecules* **2022**, *27*, e1835.
[40] M. Szarmach, E. Wagner-Wysiecka, E. Luboch, *Tetrahedron* **2013**, *69*, 10893-10905.
[41] E. Luboch, E. Wagner-Wysiecka, T. Rzymowski, *Tetrahedron* **2009**, *65*, 10671-10678.

[42] V. Deneva, A. Lyčka, S. Hristova, A. Crochet, K. M. Fromm, L. Antonov, *Dyes Pigm.* **2019**, *165*, 157-163.
[43] S. Stoyanov, L. Antonov, *Dyes Pigm.* **1989**, *10*, 33-45.
[44] L. Antonov, S. Stoyanov, *Anal. Chim. Acta* **1995**, *314*, 225-232.
[45] P. Ball, C. H. Nicholls, *Dyes Pigm*. **1982**, *3*, 5-26.
[46] L. Antonov, *Tautomerism: Concepts and Applications in Science and Technology*, Wiley-VCH, **2016.**
[47] L. Antonov, *Molecules* **2019**, *24*, e2252.
[48] Z. Neuerová, A. Lyčka, *Dyes Pigm.* **2021**, *188*, 109149.
[49] H. Rau, *Angew. Chem. Int. Ed.* **1973**, *12*, 224-235.
[50] D. Gegiou, E. Fischer, *Chem. Phys. Chem.* **1971**. *10*, 99-101.
[51] Y. Matsunaga, M. Shimane, *Bull. Chem. Soc. Jpn.* **1972**, *45*, 295-296.
[52] E. Wagner-Wysiecka, M. Szarmach, J. Chojnacki, N. Łukasik, E. Luboch, *J. Photochem. Photobiol. A* **2017**, *333*, 220-232.
[53] E. Sonego, P. Di Filippo, C. Riccardi, D. Pomata, A. Bannò, G. Simonetti, F. Buiarelli, *Food Chem.* **2023,** *409*, e135260.
[54] K. D. Pegu, *South Afr. J. Anaesth. Analg.* **2020**, *26*, S133-136.
[55] I. Krupińska, *Molecules* **2020**, *25*, e641.
[56] M. Dey, R. K. Singh, *Pharmacol. Rep.* **2022**, *74*, 439-450.
[57] B. F. Boyce, H. Y. Elder, H. L. Elliot, I. Fogelman, G. S. Fell, B. J. Junor, G. Beastall, I. T. Boyle, *Lancet* **1982,** *320*, 1009-1013.
[58] G. L. Klein, *Osteporos Sarcopenia* **2019**, *5*, 2-5.
[59] World Health Organization, *Guidelines for drinking-water quality*, Geneva, **2011**, p. 301.
[60] A. M. Skwierawska, J. F. Biernat, V. Ch. Kravtsov, *Tetrahedron* **2006**, *62*, 149-154.
[61] O. V. Dolomanov, L. J. Bourhis, R. J. Gildea, J. A. K. Howard, H. Puschmann, *J. Appl. Crystallogr.* **2009,** *42*, 339-341.
[62] G. M. Sheldrick, *Acta Cryst. A* **2015**, *71*, 3-8.
[63] G. M. Sheldrick, *Acta Cryst. A* **2008**, *64*, 112-122.
[64] J. Kožíšková, F. Hahn, J. Richter, J. Kožíšek, *Acta Phys. Slovaca* **2016**, *9*, 136-140.
[65] P. Coppens, in *Crystallographic Computing* (Ed. F. R. Ahmed, S. R. Hall, C. P. Huber), Munksgaard, Copenhagen, **1970.**
[66] M. Kyvala, I. Lukes, Program Package "OPIUM", Charles University, Prague, Czech Republic, **2000.**
[67] J. R. Lakowicz, *Principles of Fluorescence Spectroscopy, 3rd Edition*, Springer New York, New York, **2013.**
[68] C. L. Renschler, L.A. Harrah, *Anal. Chem.* **1983**, *55*, 798-800.
[69] A. Brouwer, *Pure Appl. Chem.* **2011**, *83*, 2213–2228.
[70] B. Galiński, J. Chojnacki, K. Szwarc-Karabyka, A. Małkowski, D. Sopel, A. Zwolińska, E. Wagner-Wysiecka, manuscript in preparation.
[71] M. D. Abramoff, P. J. Magalhães, S. J. Ram, *Biophotonics Int.* **2004**, *11*, 36-42.
[72] C. A. Schneider, W. S. Rasband, K. W. Eliceiri, *Nat. Methods* **2012**, *9*, 671-675.
[73] N. A. Gavrilenko, S. V. Muravyov, S. V. Silushkin, A. S. Spiridonova, *Measurement* **2014**, *51*, 464-469.
[74] S. V. Muravyov, A. S. Spiridonova, N. A. Gavrilenko, P. V. Baranov, L. I. Khudonogovo, *Instrum. Exp. Tech.* **2016**, *59*, 592-600